

CHAPTER 6

PART A: GOLD NANOPARTICLES – DOXORUBICIN HCl

PART B: GOLD NANOPARTICLES – DOXARUBICIN HCl

CHAPTER 6A: DEVELOPMENT OF GELLAN GUM REDUCED GOLD NANOPARTICLES AS A CARRIER FOR DELIVERY OF ANTICANCER DRUG, DOXORUBICIN HYDROCHLORIDE

CHAPTER 6B: DEVELOPMENT AND EVALUATION OF DOXORUBICIN HYDROCHLORIDE LOADED SOPHOROLIPID AND POLY (ETHYLENE GLYCOL) CONJUGATED GOLD NANOPARTICLES

Part A: Development of gellan gum reduced gold nanoparticles as a carrier for delivery of anticancer drug, doxorubicin hydrochloride**6A.1 Outline of the present work**

The anthracycline antibiotic doxorubicin hydrochloride (DOX) is one of the most useful antineoplastic agents. After its discovery in 1969,^[1] it has been used in the treatment of a wide variety of cancers, such as acute lymphoblastic leukemia's, multiple myeloma, carcinomas of the head and neck, breast, pancreas, stomach, liver, ovary, lung, prostate, uterus and neuroblastomas.^[2] The broad spectrum anticancer activity of DOX against various cancer cells is ensured via reactive oxygen species involving quinone group in the anthracycline ring, which is critical for generating intracellular oxidative stress, a DNA intercalating property and inhibition of topoisomerase.^[3] Despite DOX being highly effective against various malignant tumors, clinical application which involve systemic administration of the drug have demonstrated very limited efficacy in the treatment of gliomas.^[4] Moreover the cytotoxic effect of DOX lacks specificity to cancer cells and hence leads to severe side effects such as cardiotoxicity and myelosuppression.^[5] Indeed, nearly 2000 analogs have been synthesized and evaluated but very few of them have reached the stage of clinical development and approval. Second generation analogs like mitoxantrone, epirubicin or idarubicin exhibited lower cardiotoxicity, but had lower efficacy compared to the parent molecule. Hence DOX becomes indispensable when it comes to cancer chemotherapy.^[6] As DOX is a hydrophilic molecule, restricted transport is observed through the cellular membrane leading to minimal drug internalization and its ability to overcome biological barriers, such as the blood brain barrier, is rather negligible.^[7] To overcome various problems associated with DOX, many colloidal carriers have been studied with the aim of reducing cardiac toxicity and improving therapeutic efficacy.^[8] In general, the utilization of nanoparticle based vehicles as multifunctional, versatile and biocompatible carriers serve as an ideal technology as their significant advantages include the ability to target specific locations in the body, the reduction of the overall quantity of drug used at the active dosing site and the potential to reduce the concentration of the drug at healthy/unaffected sites, resulting in fewer side effects that can significantly complicate the course of treatment.^[9] In recent years, a considerable effort has been devoted to the design and synthesis of novel nanostructure materials with functional biological properties for diagnostic and therapeutic purposes. The most successful poly(ethylene glycol) liposomal nanoparticulate system for DOX till date is Doxil®^[10a] Doxil® was originally approved for the treatment of AIDS-related Kaposi's sarcoma and is now approved for use in ovarian cancer and multiple myeloma.^[10b] Recently colloidal metal nanoparticles have received substantial attention for diagnostic

and therapeutic applications. Colloidal gold nanoparticles (AuNPs) can be synthesized in sizes much smaller than micro and nanoparticles currently being tested for drug delivery applications. Moreover, unlike other polymeric based nanoparticles, AuNPs not only are smaller in size (4 to 5 nm in diameter, ~ 10³ times smaller than a bacterium) but also maintain a constant shape and size in solution.^[11] Furthermore, colloidal AuNPs are considered to be relatively inert,^[12] and can be readily conjugated to a large range of biomolecules, such as amino acids,^[13] proteins/enzymes,^[14,15] DNA^[16] and other molecular species without altering the biological activity of the conjugated species. The drugs can be grafted onto AuNPs via physical adsorption, ionic bonding and covalent bonding.^[17] The ability to modulate the surface chemistry of AuNPs, ease of surface functionalization and distinct optical properties, has spawned major interest in the utility of AuNPs for in vivo molecular imaging and therapeutic applications. All these properties of AuNPs has opened doors to wide biomedical applications encompassing colorimetric assays,^[18] cell imaging,^[19] immunostaining,^[20] biosensing^[21] and drug delivery.^[22, 23] For example, antibody- modified AuNPs displayed a million fold higher sensitivity than conventional ELISA-based assay in the detection of prostate specific antigen.^[24] Recent reports include the utilization of gold nanostructures such as gold nanoshells, gold nanocages and gold nanospheres as effective in photothermal destruction of cancer cells and tissue.^[25,26] Gold nanoparticles have also been successfully demonstrated for the delivery of peptide drug, insulin via oral and nasal route,^[27,28] enhanced antimicrobial activity against *Escherichia coli* strains^[11] and ciprofloxacin protected nanoparticles with ability to release the drug molecule over an extended period of time.^[29] The most emerging use of AuNPs is the diagnostic and therapeutic application for the treatment of cancer. Gold nanoparticles have been used for the conjugation of anticancer drug paclitaxel to increase its solubility and selectivity to cancer cells.^[30] Doxorubicin hydrochloride has also been conjugated with AuNPs and other metal nanoparticles for diagnostic and therapeutic applications. Luminescent porous silicon nanoparticles with DOX have been employed for imaging of tumors and other organs.^[31] In another study, DOX was coated on the nanodiamonds and introduced into living cells. An MTT assay was applied towards the confirmation of functional apoptosis inducing mechanisms enabled by the DOX functionalized nanodiamonds.^[9]

Despite this, very few studies have been reported regarding the possibility of applying AuNPs in drug delivery applications. The biggest obstacle is the effective loading of the drug molecules on the nanoparticle surface, their stability in physiological conditions and the drug's availability for action when needed. Here the attachment of the drug molecule through electrostatic or hydrogen bonds may be a better strategy than covalent linkages.^[17] Here in, we studied the synthesis of AuNPs using gellan gum (GG) as a reducing and capping agent, thus unraveling the superior stability they impart on the synthesized nanoparticles under various conditions. Gellan gum is characterized by many carbohydrate units and thus their capping on AuNPs should make the surface carbohydrate rich. This enables drug loading, especially for drugs that bear many hydroxyl, amine and other functional groups capable of forming hydrogen bonds. Gellan gum was used as reducing and stabilizing agent for the synthesis of AuNPs and subsequent loading of DOX. The DOX loaded AuNPs were characterized in terms of size, zeta potential, drug loading efficiency, fluorescence studies and stability studies. In addition, the cytotoxicity of the DOX-loaded AuNPs was evaluated by using two different well established glioma cell lines, that is, LN-18 and LN-229, by *in vitro* MTT assay. Immunofluorescence studies were conducted for confirmation of apoptosis induced by DOX-loaded AuNPs in the above mentioned cell lines.

6A.2 Experimental work

6A.2.1 Loading of doxorubicin hydrochloride onto gold nanoparticles

A calculated amount of DOX was added to a dispersion of GG-AuNPs, resulting in a final DOX concentration of 10^{-4} M in solution. The solution was then incubated for 24 h at room temperature and then centrifuged at 20,000 rpm for 0.5 h. The pellets thus obtained after centrifugation were separated from the supernatant solution and redispersed in milli Q water prior for further characterization. The free DOX present in the supernatant was determined by measurements of its UV absorbance and the percentage loading of DOX on AuNPs was estimated using the following formula: % Loading efficiency = [(total amount of DOX added - amount of DOX in supernatant)/total amount of DOX added] x100.

Note: Safe handling of doxorubicin was done in laminar flow hood and by wearing appropriate protective equipment such as gloves, safety glasses, masks etc.

6A.2.2 Preparation of spray dried DOX loaded gold nanoparticles

After preparation of DOX loaded gold nanoparticles (DOX-AuNPs), the dispersion was spray dried to obtain dry powder. During the spray drying operation, the inlet and outlet temperature was maintained at 100-110°C and 50-60°C respectively. The atomization air pressure and aspirator was maintained at 2 kg/cm² and -200 mmWC respectively to collect free flowing product. The product was collected and stored in desiccator till further study.

6A.2.3 Characterization

6A.2.3.A UV-Visible spectroscopy measurements

The change in the surface plasmon resonance of AuNPs, before and after loading of DOX was monitored by UV/Vis/NIR spectroscopy, carried out at a resolution of 2 nm.

6A.2.3.B Transmission electron microscopy (TEM) measurement

Samples for TEM analysis were prepared by drop casting of DOX-AuNPs and spray dried DOX loaded gold nanoparticles (SD-DOX-AuNPs) on carbon coated copper grids and allowed to dry at room temperature. Measurements were taken at an accelerated voltage of 300 kV with a lattice resolution of 0.14 nm and point image resolution of 0.20 nm. The particle size analysis was carried out using Gatan software.

6A.2.3.C Zeta potential measurements

The surface charge of AuNPs before and after loading of DOX was determined by using zeta potential analyzer. The average zeta potential of nanoparticulate dispersion was determined as such without any dilution.

6A.2.3.D pH dependent stability of doxorubicin loaded gold nanoparticles

To study the pH dependent stability of DOX-AuNPs, the DOX-AuNPs were subjected to various pH changes (pH 2-10) and then incubated for 24 h at room temperature. The analysis of the characteristic absorption peak was checked for the precipitation of DOX in AuNPs dispersion using UVA/vis spectroscopy measurements.

6A.2.3.E Fourier transforms infrared spectroscopy (FTIR) measurements

An FTIR spectrum of DOX-AuNPs was recorded in the diffuse reflectance mode at a resolution of 4 cm^{-1} in the range of $400\text{--}4000\text{ cm}^{-1}$ in KBr pellets. For comparison, FTIR spectrum of pure DOX was also recorded.

6A.2.3.F Fluorescence spectroscopy measurements

Fluorescence spectroscopy measurements were carried out to study the stability of DOX after binding with GG-AuNPs. For comparison, a fluorescence spectrum of free DOX solution was also recorded. The long term stability study of spray dried DOX-AuNPs, under stability conditions of $25^{\circ}\text{C}/65\%$ RH (room temperature) and $2\text{--}8^{\circ}\text{C}$ (refrigerated) for a period of three months, was also characterized by using fluorescence spectroscopy.

6A.2.4 In-vitro cytotoxicity assay on glioma cell lines

6A.2.4.A Cell lines and growth medium

Human glioma cell lines LN-18 and LN-229 (procured from American type culture collection, ATCC, USA) were cultured in Dulbecco's modified eagle's medium (DMEM) supplemented with 1.5 gm/L sodium bicarbonate, 4 Mm glutamine and 10% fetal bovine serum. The cultures were maintained in a humidified atmosphere of 5% CO₂ at 37°C.

6A.2.4.B Cell preparation

For cytotoxicity testing, the cells were used when they reached 60-80% confluency. The cells were diluted as needed and seeded as 4×10^3 for LN18 and 3×10^3 for LN229 in 100 μ L of media/well, sequentially plated in flat bottom 96 well plates. This number of cells was selected to avoid potential over confluence of the cells by the end of the four day experiment while still providing enough cells for adequate formazan production. After plating, the 96 well plates were then incubated for 24 h to allow adherence of the cells prior to the administration of various samples for testing.

6A.2.4.C Drug addition

After 24 h incubation at 37°C in humidified air with 5% CO₂, the culture medium was replaced with 200 μ L of fresh media containing DOX-AuNPs and free DOX solution at various concentrations (1.0 μ g/mL to 15.0 μ g/mL). To evaluate possible effect of AuNPs on cell viability, cells were also incubated with blank GG-AuNPs. Control wells containing cells received only 200 μ L of medium. After addition of all the test samples, the plates were returned to the CO incubator. The study was conducted further upto a period of 72 h to allow both time dependent and concentration dependent drug induced cytotoxicity. Furthermore, cells could be maintained in wells for this period without the need for refeeding. The antiproliferative effect of DOX was analyzed by use of MTT assay to assess the cytotoxicity of the DOX- AuNPs in comparison with free DOX and blank GG-AuNPs. The percentage cell viability was then determined. All experiments were done three times, each conditions being performed in triplicate.

6A.2.4.D MTT assay

This assay is based on the measurement of the mitochondrial activity of viable cells by the reduction of the tetrazolium salt MTT (3-(4, 5-dimethylthiazol-2-yl)-2, 5- diphenyl tetrazolium bromide) to form a blue color water insoluble product formazan.^[32] After 24 h of incubation, MTT (5 mg/mL, 20 μ L) was added to respective set of cells and the plates were incubated for an additional 4 h. After 4 h of incubation, the medium was removed and 200 μ L DMSO was added to dissolve the formazan crystals resulted from the reduction of the tetrazolium salt only by metabolically active cells. The absorbance of dissolved formazan was measured at 570 nm using a microplate reader. Since the absorbance directly correlated with the number of viable cells, the percent viability was calculated from the absorbance.

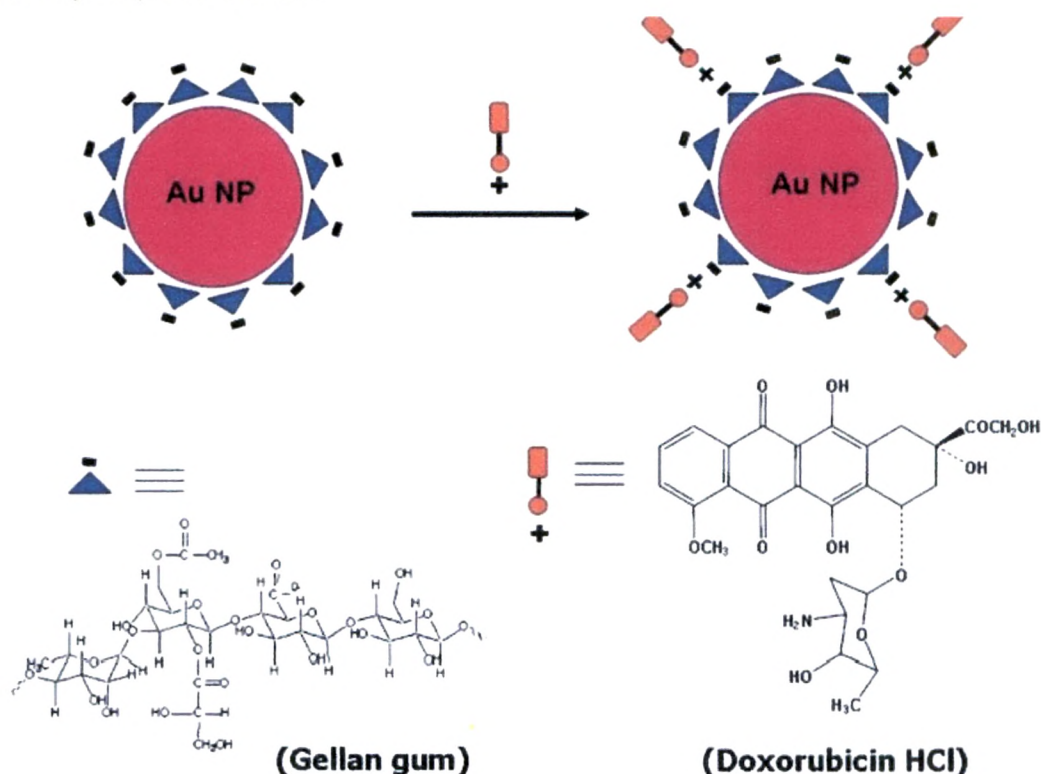
6A.2.5 Apoptosis studies using confocal laser scanning microscopy

Confocal laser scanning microscopy was used to detect the apoptotic activity of DOX on cell lines. Before addition of various formulations, LN-18 and LN-229 cells were seeded at concentration of 3×10^3 in 500 μ L of media on glass cover slips in a 24 well plate and incubated for 24 h to allow for adherence of the cells. After 24 h, when the cells were attached to the surface of the cover slips as a monolayer, culture media was replaced with different concentration of DOX-AuNPs, free DOX solution and blank GG-AuNPs (concentrations same as MTT assay). The cells were further incubated for 24 h at 37C and 5% CO₂ in a humidified environment. After incubation, the cover slips were washed extensively with ice-cold phosphate buffered saline (PBS) and fixed in 4% paraformaldehyde for 10 min at room temperature. After repeated rinses in PBS, cells were blocked in 5% BSA in PBS for 30 min at room temperature. Later the cells were again washed in PBS in dark and then the nucleus was counterstained with 4'-6-Diamidino-2-phenylindole (DAPI) for 10 min and the cells were mounted onto glass slides with 1,4-diazobicyclo-2,2,2- octanex (DABCO) as mounting medium. The cover slips were then observed using confocal microscope. The images were captured by camera coupled with microscope and processed using the computer based programmable image analyzer.

6A.3 Results and discussion

For the AuNPs to be useful as nano carrier, it has to be stable in circulatory system, yet become labile under appropriate conditions when the targeted organ is reached after administration into circulatory system.^[33] We took advantage of the biocompatible, reducing and stabilizing properties of GG for the synthesis of AuNPs. It was envisaged that this strategy would also provide sufficient exposed functional moieties on AuNPs that will aid in the subsequent attachment of large number of biomolecules for drug delivery applications (Scheme 6A.1).

After synthesis of stable GG-AuNPs, the loading of DOX onto the nanoparticles was studied. Based on the UV/Vis absorbance studies, the loading efficiency of DOX on GG-AuNPs was determined to be 75%. Because the GG-AuNPs were negatively charged and DOX ions (NH_3^+) were cationic, the interaction between the AuNPs and DOX appeared to be straightforward. Huang et al., studied the loading of DOX molecules on nanodiamonds^[9] and found the addition of salt such as NaCl to be a necessary component of the loading process. In case of GG-AuNPs, the positively charged DOX molecules were bound to the negatively charged GG-AuNPs surface by electrostatic forces by simple incubation.



Scheme 6A.1: Schematic diagram showing anionic gellan gum gold nanoparticles and subsequent loading of cationic doxorubicin hydrochloride on gold nanoparticles.

At neutral pH, the zeta potential of GG (pKa = 3.1) reduced AuNPs (0.02% w/v) was -38.25 mV. This clearly indicated that the AuNPs were wrapped with the anionic GG which helped nanoparticles to remain electrostatically stable. The zeta potential of DOX (pKa = 8.2) loaded AuNPs was -30.00 mV. The decrease in the zeta potential was ascribed to the presence of positively charged DOX on GG-AuNPs. The little decrease in the charge even at 75% loading of DOX indicates that other attractive forces including hydrogen bonding could be playing a major role facilitating the drug loading process. It was clear that even after DOX loading, GG-AuNPs remained in suspension by their electrostatic repulsion and maintained the negative charge on the surface. The hydrogen bonding hypothesis between protonated amine group of DOX molecule with GG on the surface of AuNPs was also supported by FTIR; N-H stretching of the pure DOX at 3777 cm^{-1} was shifted to 3372 cm^{-1} in case of DOX- AuNPs (Figure 6A. 1).

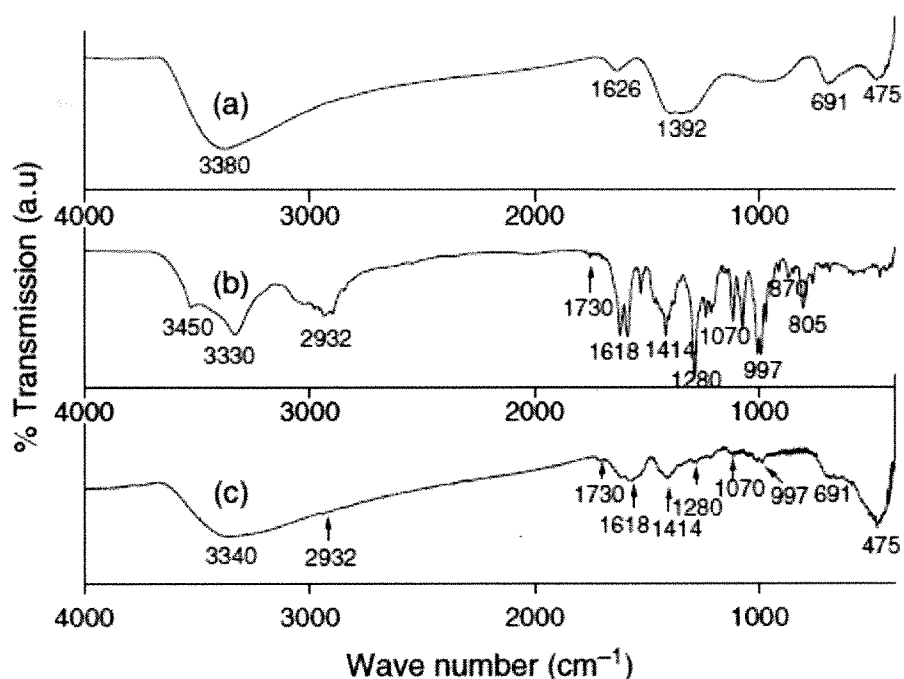


Figure 6A.1: FTIR spectra of (a) Gold nanoparticles (b) pure doxorubicin solution and (c) doxorubicin loaded gold nanoparticles.

We studied the pH dependent stability of DOX loaded nanoparticles by adjusting the pH of the DOX-AuNPs dispersion between pH 2 to 10 (Figure 6A. 2). It was observed that the DOX-AuNPs were very stable between pH 4.0 to 8.0. Below pH 4.0 and above 8.0, the addition of DOX solution in the colloidal AuNPs caused the particles to aggregate. The retention of absorbance intensity corresponding to DOX d that the drug was stable in this pH window.

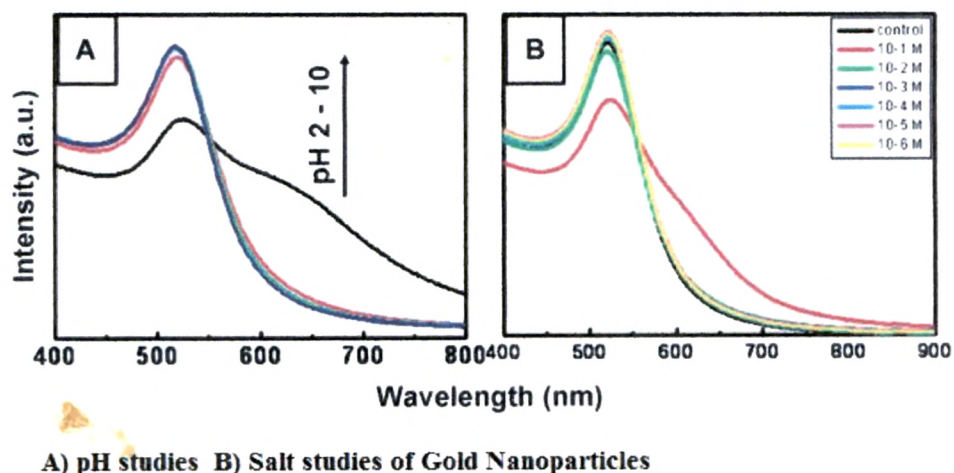


Figure 6A.2: UV-Vis absorption spectra of pH study of doxorubicin loaded gold articles.

This was an important exercise because stable particles would show better uptake and subsequent bioavailability as aggregation would be undesirable and may compromise the uptake as well as activity.^[34] The TEM images recorded from the DOX-AuNPs [Figure 6A. 3(a)] indicated that the overall structure of the nanoparticles and their assemblies were not different in comparison to blank GG- AuNPs.

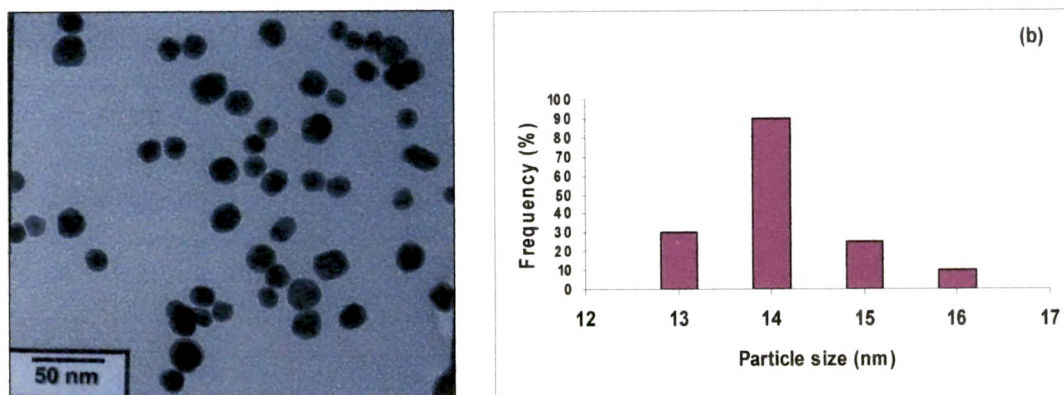


Figure 6A.3: (a) TEM image of doxorubicin loaded gold nanoparticles (reduced by 0.02% w/v gellan gum) and (b) particle size distribution of the same.

The TEM image of DOX-AuNPs retain their morphology giving credence to the assertion that DOX loading neither cause much change in their size nor lead to any aggregation. When DOX molecules are conjugated to GG-AuNPs, they can serve as the protector of AuNPs and thereby avoid aggregation of AuNPs. The particle size distribution of DOX-AuNPs [Figure 6A. 3(b)] revealed that the average size of the nanoparticles was 14 nm. There was no significant change in the particle size before and after loading of DOX on GG-AuNPs. We further used spray drying to prepare powdered DOX-AuNPs. The SD-DOX-AuNPs were free flowing without any aggregation or change in color. The SD-DOX-AuNPs were further redispersed in water and evaluated for any change in morphology and stability after spray drying. The TEM image [Figure 6A.4 (a)] showed that the overall assemblies of the DOX- AuNPs were not affected after spray drying. There was no change in the shape and size of the nanoparticles. The particle size distribution of SD-DOX-AuNPs [Figure 6A.4 (b)] revealed that the average size of nanoparticles was also 14 nm. The average particle size did not change in comparison to DOX loaded GG-AuNPs. The TEM and particle size distribution concluded that the SD-DOX-AuNPs formed after spray drying retained all the properties of nanoparticles, with no change in shape, size and without aggregation. Thus the drug loaded nanoparticles can be stored in powder form and redispersed whenever required.

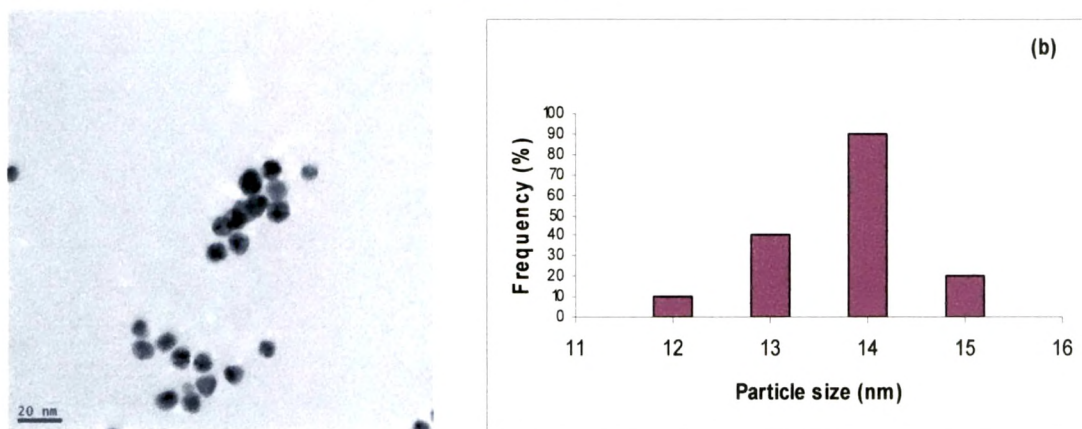


Figure 6A.4: (a) TEM image of spray dried doxorubicin loaded gold nanoparticles and (b) particle size distribution of the same.

The binding and stability of DOX molecule after loading on AuNPs was studied using fluorescence spectroscopy. Fluorescence studies offer an excellent probe for confirming the binding of drug molecule with AuNPs. It has been previously reported that gold metal efficiently quenches the emission of many fluorophores.^[35] Doxorubicin hydrochloride exhibits a unique fluorescence emission spectrum that is susceptible to changes in its microenvironment.^[36] The emission spectra of DOX solution and DOX-AuNPs were recorded from 490 to 800 nm at a fixed excitation of 480 nm. The fluorescence emission spectra recorded are shown in figure 6A. 5. There was no major change in the spectral profile in DOX loaded AuNPs and the peaks at 597 nm and 635 nm that were observed in pure DOX were retained. Doxorubicin hydrochloride was initially highly fluorescent but with the addition of AuNPs, the fluorescence intensity was reduced and this quenching of intensity could be attributed to the electrostatic or hydrogen bond formation between the DOX molecule and AuNPs, which was responsible for the decrease of fluorescence. Moreover, the preservation of the fluorescence signature supports the claim that DOX structure was retained following complexation with nanoparticles,^[37] which is important for the biological activity of the DOX molecule.

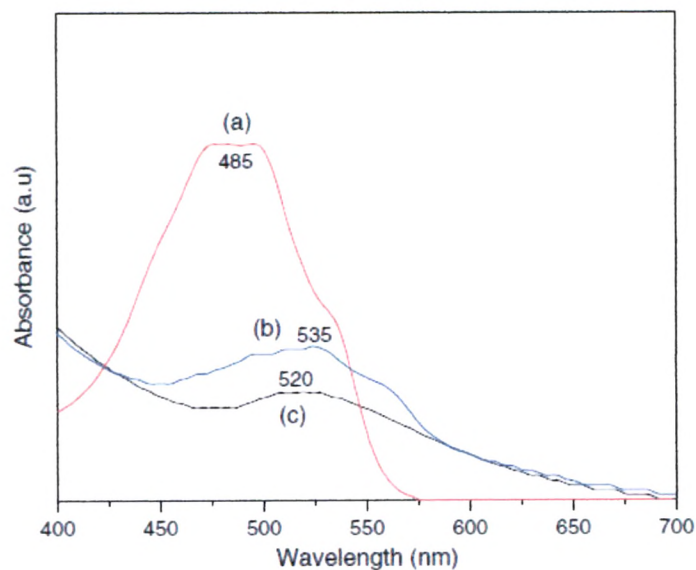


Figure 6A.5: UV Spectra & Figure 6A.6 Fluorescence spectra of (a) doxorubicin solution and (b) doxorubicin loaded gold nanoparticles.

UV Spectra of (a) pure Doxorubicin (b) Doxorubicin attached to gold nanoparticles (c) Gold nanoparticles –Peak is broadened and red shifted at 535 nm upon addition of colloidal gold to doxorubicin

Fluorescence spectroscopy was also used to evaluate the stability of spray dried DOX-AuNPs, monitored over a period of three months (Figure 6A.6). It was found that the spray dried powder was stable at both storage conditions of 2-8°C (refrigerated) and 25°C/65% RH (room temperature), during its storage for 3 months.

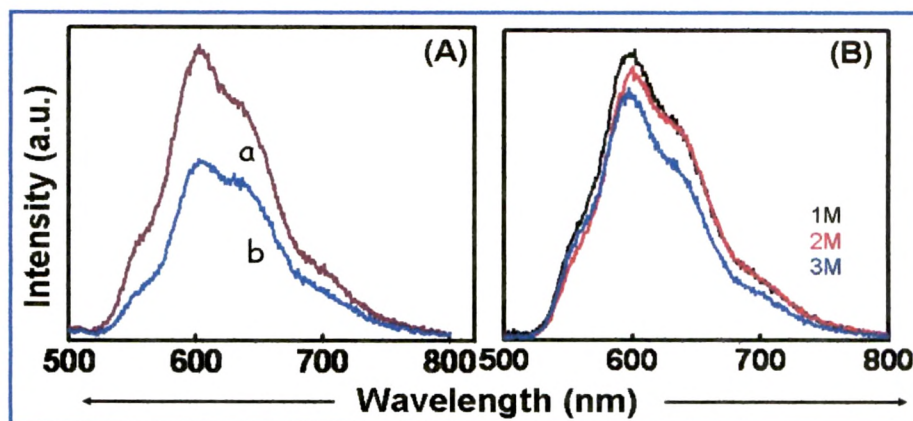


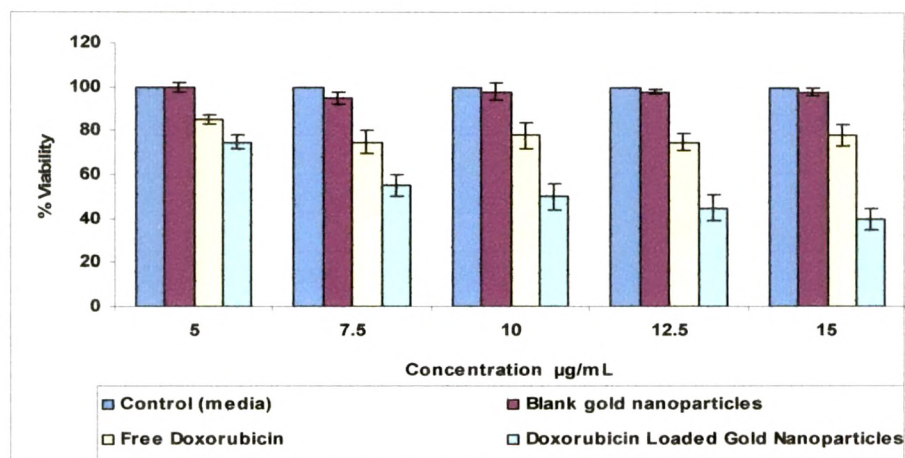
Figure 6A.6: Fluorescence spectra of spray dried doxorubicin loaded gold nanoparticles, stability period of three months, (a) 2-8°C (refrigerated) and (b) 25°C/65% RH (room temperature).

There was no change in the fluorescence spectra profile of SD-DOX-AuNPs in comparison to plain DOX solution. The decrease in the intensity in 3rd month can be attributed to quenching in fluorescence in the presence of AuNPs.

To explore the platform capabilities of the AuNPs drug carrying technology, we determined the cytotoxic effect of GG-AuNPs as well as the sensitivity of DOX loaded AuNPs on human glioma cell lines. Brain tumors, especially malignant gliomas, belong to the most aggressive brain tumors in adults.^[38,39] Despite DOX clinical effectiveness in the treatment of many malignant tumors, clinical trials involving systemic administration of the drug have demonstrated very limited efficacy in the treatment of gliomas.^[40] Very high doses of DOX must be administered systemically to exert any therapeutic benefit and these doses are highly toxic and therefore ineffective in treating CNS malignancies.^[41] The cytotoxicity of different formulations namely, free DOX solution, DOX loaded AuNPs, control AuNPs and only culture media, was evaluated on human glioma cell lines (LN-18 and LN-229) using *in-vitro* MTT assay. The wells that received only media were regarded as a control with a cell viability of 100%. No cytotoxicity effect of GG-AuNPs was observed on either cell lines as the cell viability did not decrease even after 48 h of experiment. It showed that the AuNPs were well tolerated by both cell lines and had no effect on cell viability, which further confirmed the biocompatibility of the AuNPs.^[12] Figure 6A.7 showed the percent viability of LN-18 cell line after exposure to DOX, in pure

solution form and as loaded on AuNPs for 24 and 48 h respectively. Each concentration of the drug loaded AuNPs was taken such that the DOX concentration was similar to that in free solution making a direct comparison possible. At the end of 24 h, none of the concentration of pure DOX solution caused 50% inhibition of the cell growth, whereas DOX loaded AuNPs exhibited strongly enhanced cytotoxicity, with viability ranging from about 50% at 7.5 $\mu\text{g/mL}$ to 40% at 15.0 $\mu\text{g/mL}$ [Figure 6A. 7(a)], After 48 h of incubation [Figure 6A. 7(b)], all the LN-18 cells cultured in the presence of DOX-AuNPs within the checked concentration range (5.0 $\mu\text{g/mL}$ to 15.0 $\mu\text{g/mL}$) showed more significant reduction in viability. The highest concentration at 15.0 $\mu\text{g/mL}$ was able to decrease the cell viability to 5% at the end of 48 h. The maximum decrease in cell viability achieved via 15.0 $\mu\text{g/mL}$ free DOX solution was 40% at the end of 48 h indicating a slower rate of decrease (50% to 40%) as compared to the DOX-AuNPs (40% to 5%).

(a)



(b)

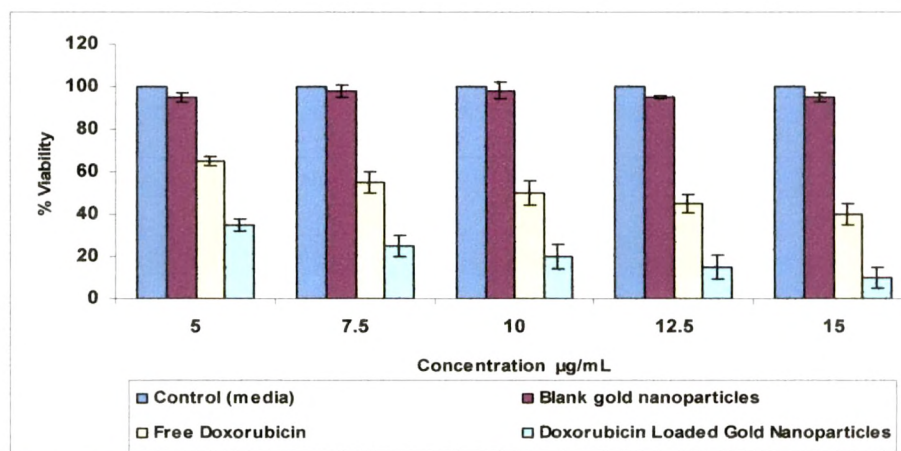
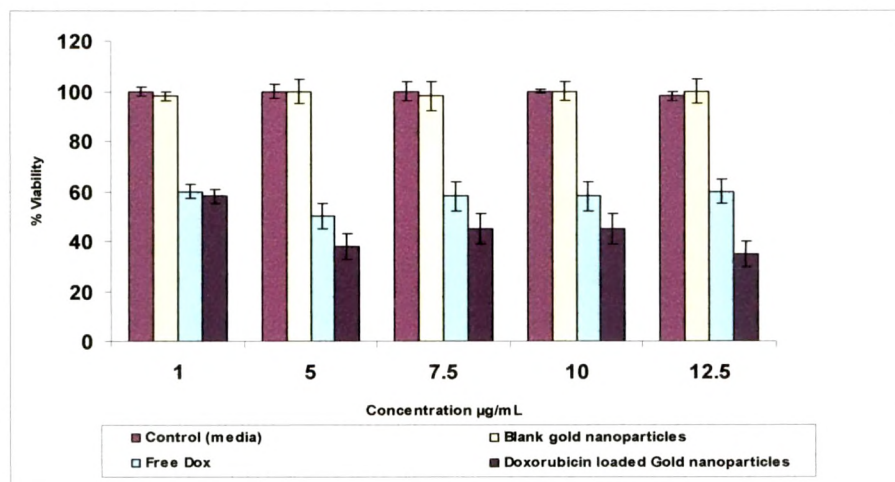


Figure 6A.7: Viability of LN-18 after (a) 24 and (b) 48 h, after exposure to (from left to right): control (media), blank gold nanoparticles, doxorubicin solution and doxorubicin loaded gold nanoparticles.

In case of human glioma cell line LN-229 (Figure 6A. 8), free DOX solution and DOX-AuNPs gradually increase their cytotoxicity with increasing concentration and the cytotoxicity was dominated by DOX-AuNPs. At the end of 24 h incubation [Figure 6A. 8(a)], the decrease in cell viability via free DOX solution and DOX- AuNPs at the concentrations range studied (1.0 $\mu\text{g}/\text{mL}$ to 12.5 $\mu\text{g}/\text{mL}$) was between 58-51% and 57-34% respectively.

(a)



(b)

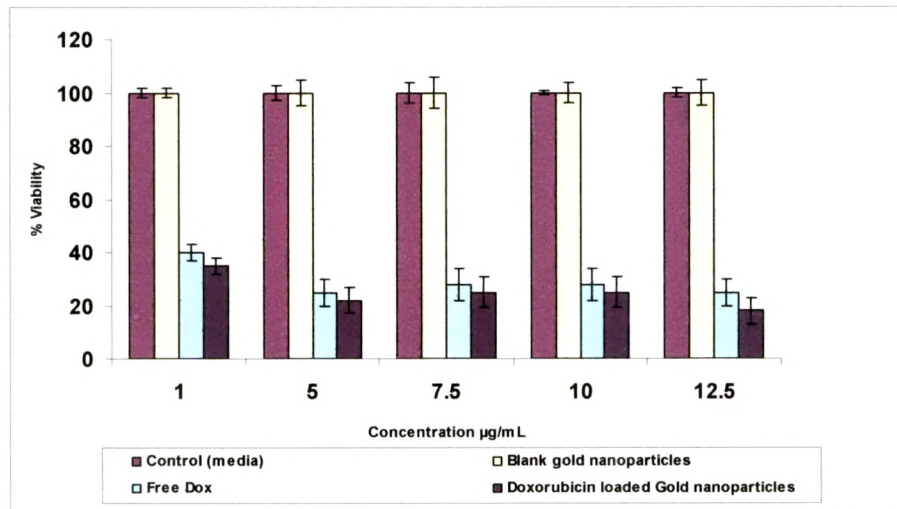


Figure 6A.8: Viability of LN-229 after (a) 24 and (b) 48 h, after exposure to (from left to right): control (media), blank gold nanoparticles, doxorubicin solution and doxorubicin loaded gold nanoparticles.

At the end of 48 h incubation [Figure 6A. 8(b)], the decrease in cell viability at highest concentration of 12.5 $\mu\text{g/mL}$ was dominated by DOX-AuNPs, as the cell viability reduced to 10% compared to 24% in the case of free DOX solution. Many authors studied the incorporation of DOX in colloidal carriers. The increase of DOX cytotoxicity compared to the solution has already been observed with polymeric nanoparticles, micelles and liposomes carrying DOX.^[42] The AuNPs employed here also turn out to be very effective DOX carriers as compared to the intricate systems mentioned above. In our study, we observed a steep increase in the cytotoxicity in both the cell lines when AuNPs loaded with DOX was used. A possible explanation for the activity enhancement of DOX loaded AuNPs is that the DOX carried by the AuNPs inside the cells results in higher cytotoxicity, where as free DOX is released outside the cells. This improved internalization of DOX loaded AuNPs is by an endocytosis mechanism compared to passive diffusion mechanism of free DOX into cells.^[43] Moreover, it was found that binding of DOX to nanoparticles increased the efficacy against glioma tumors.^[39]

We next analyzed the kind of death DOX loaded AuNPs caused on glioma cell lines. Doxorubicin hydrochloride is known to induce apoptosis (i.e., programmed death of tumor cells) by blocking the cell cycle and inhibiting the DNA polymerase enzyme.^[44] The apoptosis induced cells exhibit a number of characteristics including cell shrinkage, condensation of chromatin, nuclear fragmentation and appearance of apoptotic bodies.^[45] Interactions of DOX loaded AuNPs with glioma cells were imaged by using confocal microscope to assess the impact of DOX loaded AuNPs on cellular morphology/architectures. After incubation of human glioma cell lines LN-18 and LN-224 with DOX loaded AuNPs for 24 h, the morphology of both cell lines changed significantly (Figure 6A. 9 &10). The blank AuNPs treated cells had no change in their morphology and the free DOX treated cells did not show major apoptosis bodies. It was possible to visualize DOX directly since DOX (red color) itself is a fluorescent molecule.

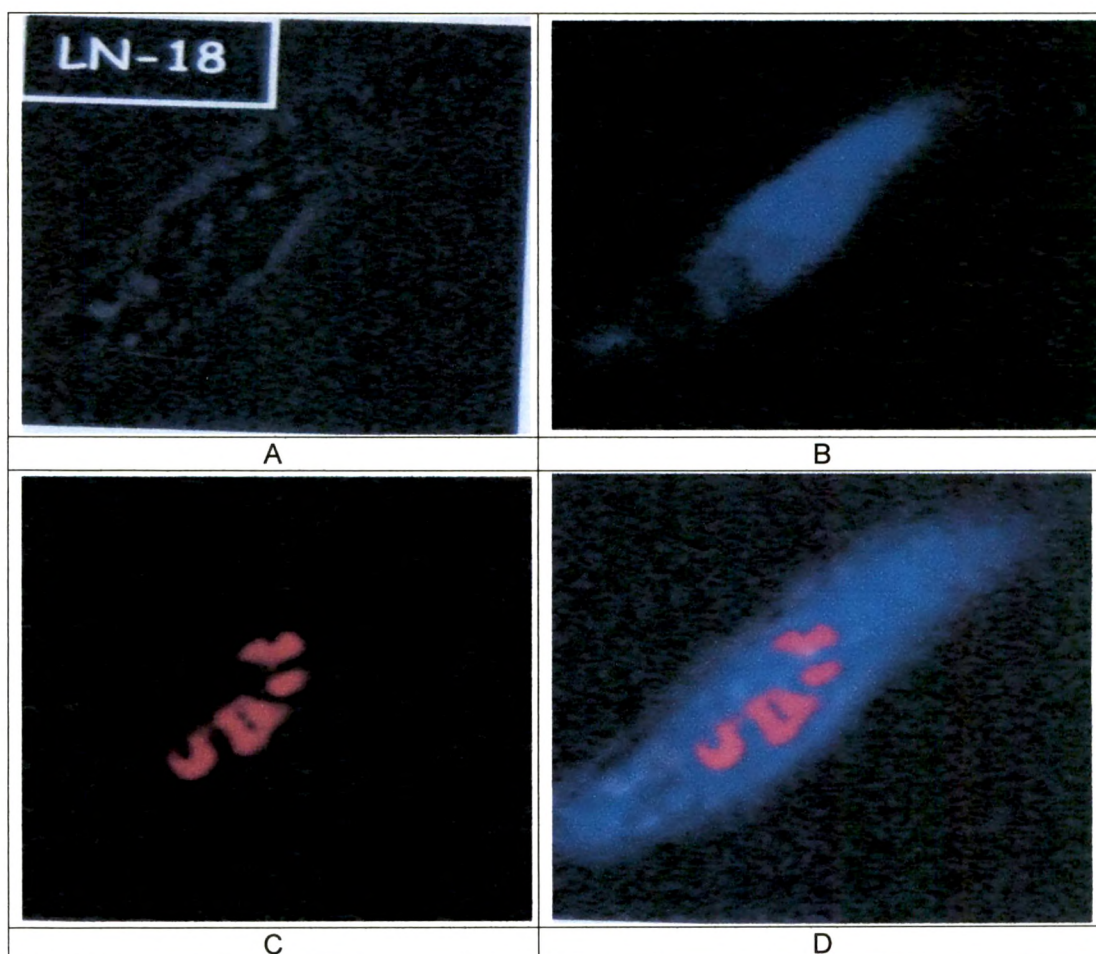


Figure 6A.9: Confocal microscopy images to demonstrate the apoptosis induced by doxorubicin loaded gold nanoparticles on human glioma cell line LN-18 (a) Phase (b) DAPI (c) doxorubicin loaded gold nanoparticles and (d) overlaid (b&c).

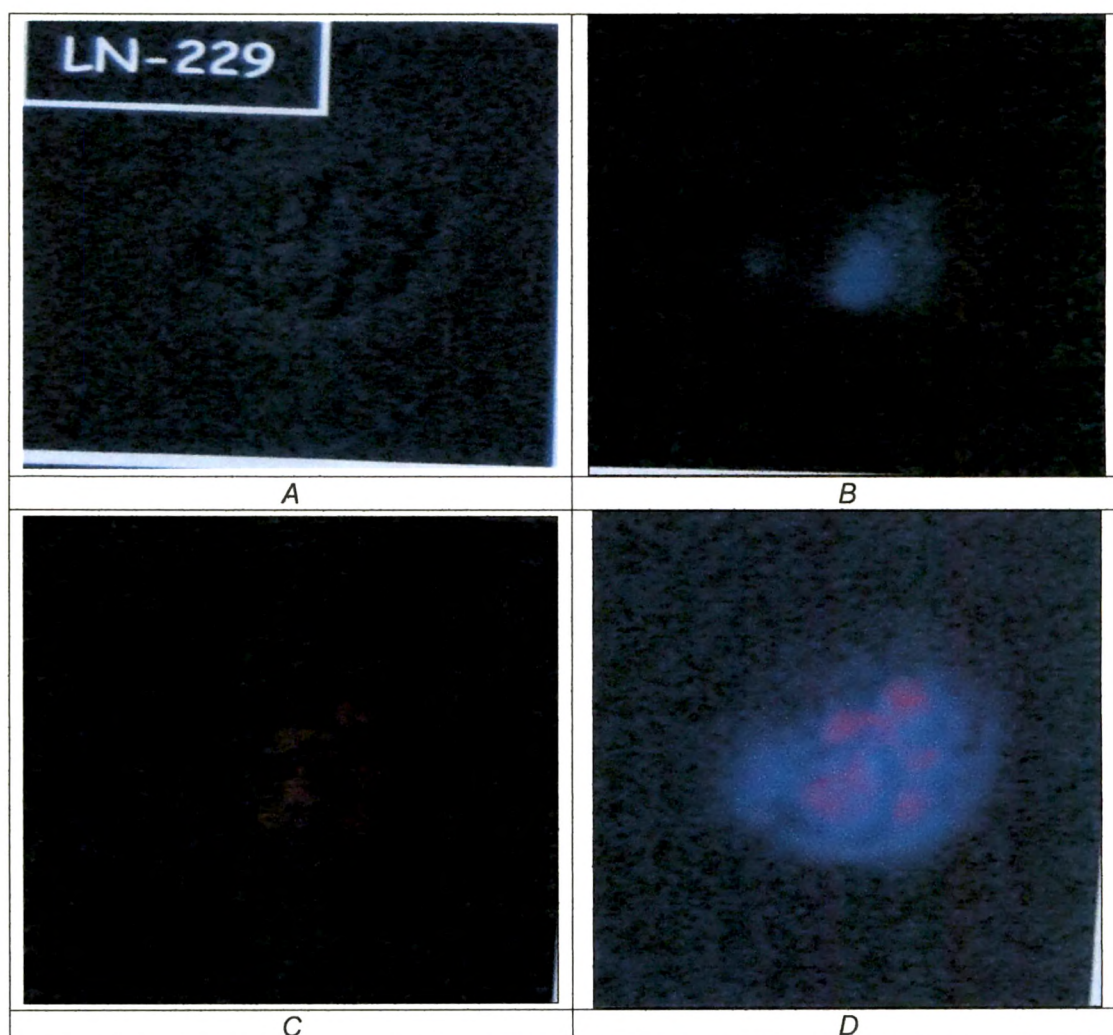


Figure 6A.10: Confocal microscopy images to demonstrate the apoptosis induced by doxorubicin loaded gold nanoparticles on human glioma cell line LN-229 (a) DAPI (c) doxorubicin loaded gold nanoparticles and (d) overlaid (b&c).

The apoptosis induced by DOX-AuNPs was clearly visible as the cells shrunk to spherical shape and most of the cells were detached from the cover slip. The cytoplasm of the cell was distributed badly and formed the apoptotic bodies and some of the cells were budding. Because of apoptosis, most of the cells were detached from the cover slips and washing further removed the apoptotic cells but the main apoptosis features like cell shrinkage, chromatin condensation and nuclei fragmentation were clearly observed with the help of confocal microscopy. Confocal images clearly demonstrated the apoptosis induced cell death by DOX loaded AuNPs on human glioma cell lines LN-18 and LN-229.

PART B: DEVELOPMENT AND EVALUATION OF DOXORUBICIN HYDROCHLORIDE LOADED SOPHOROLIPID AND POLY(ETHYLENE GLYCOL) CONJUGATED GOLD NANOPARTICLES

6B.1 Outline of the present work

In continuation of our quest for the bio-mediated synthesis of AuNPs and their application as carrier for the delivery of biomolecules, we studied the surface functionalization of gellan gum reduced gold nanoparticles by using microbial produced biosurfactant "Sophorolipid". The yeast cells such as *Candida bombicola*, *Yarrowia lipolytica*, *Candida apicoia* and *Candida bogoriensis* when challenged with fatty acids plus glucose (oleic acid, stearic acid, etc) results in the formation of glycolipids, known as sophorolipids (SL).^[46] First described by Tulloch^[47] in 1961, SL are generally present in the form of disaccharide sophoroses linked glycosidically to the hydroxyl group at the penultimate carbon of fatty acids. They mainly occur as mixtures of close ring (macrolactone form) and open ring (acidic form) structures, which undergo acetylation to various extends at the primary hydroxyl group of the sophorose ring.^[48,49] Sophorolipid themselves have shown to possess very interesting biological and other applications. Sophorolipids have good surfactant properties that have been used in petroleum industry and in food areas as emulsifiers.^[50] Sophorolipids and their derivatives have shown immense potential application as therapeutic agents that can function in cosmetic as a high value isturizer,^[51] as antibacterial, antiviral, spermicidal and antifungal agents.^[52-56] In addition to the above, reports have also indicated the therapeutic application of SL as immunomodulators for the treatment of septic shock^[57] and most importantly as anticancer agent.^[58-60] From the literature, it is clear that SL and several of the modified analogues have been extensively investigated by various groups. Manasi et. al., studied the SL obtained from oleic acid as capping agent for cobalt nanoparticles.^[61] Sanjay et al., studied the reducing/capping agent properties of SL derived from oleic acid for the synthesis of water dispersible silver nanoparticles.^[62]

But still their application in nanoparticulate and cancer therapy has yet not been fully explored. Gliomas are highly vascularized, aggressive and diffusely infiltrating primary brain tumor that are rarely, if ever, cured, despite advances in modern chemo and radiotherapy.^[63] The failure of typical cytotoxic therapies to cure cancer has been attributed to the fact that they target rapidly proliferating tumor cells, while sparing the tumor stem cell compartment, which has a low proliferation rate and high tumorigenic potential.^[63] We initiated our explorations by synthesizing AuNPs by using gellan gum (GG) and subsequent loaded anticancer drug, DOX. The cytotoxicity of the DOX loaded AuNPs was evaluated against two different human glioma cell lines, that is, LN-18 and LN-229, by in vitro cytotoxicity assay (Part 6A). After attaining success in decreasing the viability of both human glioma cells, we thought of utilizing the same nanoparticles to test out if they can demonstrate any effect against human glioma stem cell. The human glioma stem cell line evaluated was HNGC-2. The DOX loaded GG-AuNPs were not as effective against human stem cells lines compared to other human glioma cell lines. The reason behind this may be that cancer stem cells mainly resist current drug therapies and repair DNA after radiation treatment more efficiently than their differentiated, daughter cells. That explains why solid tumors often recur after treatment and the new tumors are much harder to treat.^[64]

For any targeted biomedical applications, surface functionalization of AuNPs is essential in order to target them to specific disease areas and allow them to selectively interact with cells or biomolecules. Properly functionalized AuNPs not only can serve as a drug reservoir, but also provide a long circulation time and low cytotoxicity; thus, they have emerged as attractive candidates for delivering various payloads into their targets.^[65] So, here by taking the advantage of surfactant and anticancer properties of SL, we used it for surface functionalization of gellan gum reduced gold nanoparticles (SL-AuNPs). Moreover, SL-AuNPs could also cross BBB (owing to the presence of specific targeting moieties) and will help to deliver drugs either electrostatically or covalently attached to them. Here in we describe our results disclosing the efficient manipulation of human glioma cell line as well as human glioma stem cell line by SL conjugated AuNPs and the doxorubicin hydrochloride loaded SL-AuNPs. The combine use of DOX and SL with AuNPs may help in increasing the efficacy of the treatment against human glioma cells and stem cells, without increasing the toxicity.

Additionally, another approach was adopted for surface modification of SL-AuNPs by the use of Poly (ethylene glycol), (PEG). Surface modification of nanoparticles with water soluble PEG, which has been approved for human intravenous application, helped in stabilization of nanoparticles by steric repulsion to inhibit colloid aggregation in physiological conditions.^[66] Due to the high degree of hydration and randomly coiled PEG molecules, it is reported that the drug molecules could be shielded from being uptaken by the reticuloendothelial system (RES).^[67] Surface modification of nanoparticles through the PEG spacer would, therefore, allow the modified nanoparticles to remain for extended duration in the systemic circulation and provide flexibility to the attached ligand for efficient interaction with its target.^[68] The PEG has been used extensively for surface modification on AuNPs in order to achieve excellent stability and conjugation with biomolecules. Wang et al., studied the PEG modified synthesis of AuNPs, size of particles were found to decrease with increasing PEG concentration, moreover PEG (MW6000) was found optimal for size control and colloidal stability in biologically relevant media.^[69] Niidome et al., reported modification of gold nanorods by preparing them in hexadecyltrimethylammonium bromide (CTAB) solution using thiolated PEG. Poly(ethylene glycol) modified AuNPs were found in blood at 0.5 h after i.v. injection, whereas most of gold was detected in the liver in the case of original gold nanorods stabilized with CTAB.^[70] Similarly reports indicated that for therapeutic applications, where AuNPs are used as carrier for drug delivery, PEG molecules are insulated on AuNPs before loading of drug molecules to achieve higher stability and conjugation to biomolecules.^[71-73] But recent reports have raised concern about use of PEG in association with AuNPs as drug delivery carriers. Cho et al., reported an *in vivo* toxicity study using 13 nm sized AuNPs coated with PEG (MW 5000). The studies indicated that the 13 nm sized PEG coated AuNPs were seen to induce acute inflammation and apoptosis in the liver of the mouse.^[74] The results suggested that careful scrutiny of the *in vitro* and *in vivo* toxicities of PEG- AuNPs nanoparticles are required that have been previously shown to have limited or no toxicity at the cellular level. We thought it will be interesting to study the effect of PEG conjugation on sophorolipid gold nanoparticles (PEG-SL-AuNPs). The doxorubicin hydrochloride was also loaded on PEG-SL-AuNPs, and the cytotoxicity of PEG-SL-AuNPs and DOX-PEG-SL-AuNPs was evaluated on human glioma cell line LN-229 and human glioma stem cell line HNGC-2.

6B.2 Experimental work

6B.2.1 Conjugation of sophorolipid and Poly (ethylene glycol) on gold nanoparticles

After synthesis of GG-AuNPs, AuNPs dispersion was thoroughly dialyzed (dialysis tubing 12 kDa cut off) for 24 h to remove the by products of the reaction. Sophorolipid (10^{-4} M) was added to the GG-AuNPs dispersion under stirring. The stirring was continued for 24 h to ensure optimum conjugation of SL on GG-AuNPs. For conjugation of PEG, 0.2% w/v solution of PEG was added to SL-AuNPs under continuous stirring. The surface plasmon resonance of SL-AuNPs and PEG-SL AuNPs was monitored using UV/Vis spectroscopy.

6B.2.2 Loading of doxorubicin hydrochloride onto sophorolipid and Poly(ethylene glycol) conjugated gold nanoparticles

A calculated amount of DOX was added to a dispersion of SL-AuNPs and PEG-SL-AuNPs, obtained as described above, resulting in a final DOX concentration of 10^{-4} M in solution. The solution was then incubated for 24 h at room temperature and then centrifuged at 20,000 rpm for 0.5 h. The pellets thus obtained after centrifugation were separated from the supernatant solution and redispersed in milli Q water prior to further characterization. The free DOX present in the supernatant was determined by measurements of its UV absorbance and the percentage loading of DOX on SL-AuNPs and PEG-SL-AuNPs was estimated by following formula: % Loading efficiency = [(total amount of DOX added - amount of DOX in supernatant)/total amount of DOX added] x100.

6B.2.3 Preparation of spray dried sophorolipid, Poly (ethylene glycol) conjugated and doxorubicin loaded sophorolipid and Poly (ethylene glycol) conjugated gold nanoparticles

After preparation of SL-AuNPs, PEG-SL-AuNPs and DOX loaded SL-AuNPs and PEG-SL-AuNPs, the dispersions were spray dried to obtain dry powder. During the spray drying operation, the inlet and outlet temperature was maintained at 100- 110°C and 50-60°C respectively. The atomization air pressure and aspirator was maintained at 2 kg/cm² and - 200 mmWC respectively to collect the dry and free flowing products. The products were collected and stored in desiccator till further study.

6B.2.4 Characterization

6B.2.4.A UV-Visible spectroscopy measurements

The change in the surface plasmon resonance of SL- AuNPs and PEG-SL-AuNPs after conjugation with GG-AuNPs was monitored by UV/Vis/NIR spectrophotometer, operated at a resolution of 2 nm.

6B.2.4.B Transmission electron microscopy (TEM) measurement

Samples for TEM analysis were prepared by drop casting of as such dispersions and spray dried SL-AuNPs, PEG-SL-AuNPs, DOX loaded SL-AuNPs and PEG-SL- AuNPs on carbon coated copper grids and allowed to dry at room temperature, Measurements were taken at an accelerated voltage of 300 kV with a lattice resolution of 0.14 nm and point image resolution of 0.20 nm. The particle size analysis was carried out using Gatan software.

6B.2.4.C Zeta potential measurements

The surface charge of SL-AuNPs and PEG-SL-AuNPs before and after loading of DOX was determined using a zeta potential analyzer. The average zeta potential of nanoparticulate dispersion was determined as such without any dilution.

6B.2.4.D In vitro stability studies of sophorolipid and Poly (ethylene glycol) conjugated gold nanoparticles

The stability of SL-AuNPs and PEG-SL-AuNPs was studied over time and under different pH and electrolytic conditions. In case of pH studies, the pH of SL-AuNPs and PEG-SL-AuNPs was adjusted between pH 2-12 and incubated for 24 h at room temperature. The analysis of the characteristic absorption peak was checked for the precipitation of AuNPs. The stability of SL-AuNPs and PEG-SL-AuNPs was also tested by challenging the AuNPs in the presence of electrolyte (sodium chloride) solution and incubated for 24 h before taking the absorption measurements. For long term stability study, the spray dried SL-AuNPs and peg-sl-aunps were kept at 25°C/65% rh (room temperature) and at 2-8°C (refrigerated) for a period of six months.

6b.2.4.E fluorescence spectroscopy measurements

Fluorescence spectroscopy measurements were carried out to study the stability of dox after binding with sl-aunps and PEG-SL-AuNPs. A fluorescence spectrum of free DOX solution was also recorded. The stability study of spray dried DOX loaded SL-AuNPs and PEG-SL-AuNPs for a period of three months were also monitored by fluorescence spectroscopy.

6B.2.5 In-vitro cellular uptake and cytotoxicity assay

6B.2.5.A Cell lines and growth medium

For uptake studies, human glioma cell line LN-229 was used. For cytotoxicity studies, human glioma cell lines LN-229 and human glioma stem cell line HNGC-2 were used. LN-229 cell line was procured from American type culture collection, ATCC, USA and HNGC-2 was developed at National Center for Cell Sciences, Pune, India. The cells were cultured in dulbecco's modified eagle's medium (DMEM) supplemented with 1.5 grrf1 sodium bicarbonate, 4 Mm glutamine and 10% fetal bovine serum. The cultures were maintained in a humidified atmosphere of 5% CO₂ at 37°C.

6B.2.5.B Synthesis of Texas red labeled sophorolipid and Poly (ethylene glycol) conjugated gold nanoparticles

The dialyzed SL-AuNPs and PEG-SL-AuNPs were labeled by addition of excess Texas red (140 ng/μL in DMSO). The colloidal dispersion was incubated overnight in darkness at 4C to avoid photo degradation of Texas red molecules. Free Texas red in the AuNPs dispersion was removed by centrifugation at 10,000 rpm for 10 min followed by washings with carbonate buffer (pH 8.4). This effectively removed any loosely bound Texas red to the nanoparticles. The pellets containing Texas red labeled SL-AuNPs and PEG-SL-AuNPs were redispersed in carbonate buffer and used for further studies. The amount of carbonate buffer in which the pellets were redispersed was adjusted such that the surface plasmon peak intensity of the AuNPs dispersion obtained before and after centrifugation was same.

6B.2.5.C Cell preparation

For uptake of SL-AuNPs and PEG-SL-AuNPs, the cells were seeded at concentration of 3×10^3 in 500 pL of media on glass cover slips in a 24 well plate and incubated for 24 h to allow for adherence of the cells. For cytotoxicity testing, the cells were utilized when they reached 60-80% confluent. The cells were diluted as needed and seeded as 3×10^3 for LN229 and HNGC-2 in 100 μL of media/well, sequentially plated in flat bottom 96 well plates. This number of cells was selected to avoid potential over confluence of the cells by the end of the four day experiment while still providing enough cells for adequate formazan production. After plating, the 96 well plates were then incubated for 24 h to allow adherence of the cells prior to the administration of various samples for testing. For apoptotic studies, before addition of various formulations, LN-229 cells and HNGC-2 were seeded at concentration of 3×10^3 in 500 [μL of media in 24 well plates on cover slips and grown for 24 h to achieve semi-confluent cultures.

6B.2.5.D Sample addition

For cellular uptake, after 24 h of incubation, when the cells were attached to the surface of the cover slips as a monolayer, culture medium were replaced with 500 μ L of solution containing fresh medium and Texas red labeled SL-AuNPs and PEG- SL-AuNPs. The cells were further incubated for 24 h at 37°C and 5% CO₂ in a humidified environment. For cytotoxicity testing, after 24 h incubation at 37°C in humidified air with 5% CO₂, the culture medium were replaced with 200 μ L of fresh media containing SL-AuNPs, PEG-SL-AuNPs, DOX-SL-AuNPs, DOX-PEG-SL- AuNPs and free DOX solution at various concentrations (1.0 μ g/mL to 12.5 μ g/mL). Control wells containing cells received only 200 μ L of medium. After addition of all the test samples, the plates were returned to the CO₂ incubator. The study was conducted further upto a period of 72 h to allow both time dependent and concentration dependent drug induced cytotoxicity. The MTT assay was used to assess the cytotoxicity of the SL-AuNPs and PEG-SL-AuNPs on glioma cell lines. The cytotoxicity of DOX-SL-AuNPs and DOX-PEG-SL-AuNPs was also evaluated in comparison to free DOX solution. The percentage cell viability was then determined. All experiments were done three times, each condition being performed in triplicate. For apoptotic activity, when the cells were attached to the surface of the cover, they were incubated with DOX-SL-AuNPs and DOX-PEG-SL- AuNPs. The cells were further incubated for 24 h at 37°C and 5% CO₂ in a humidified environment.

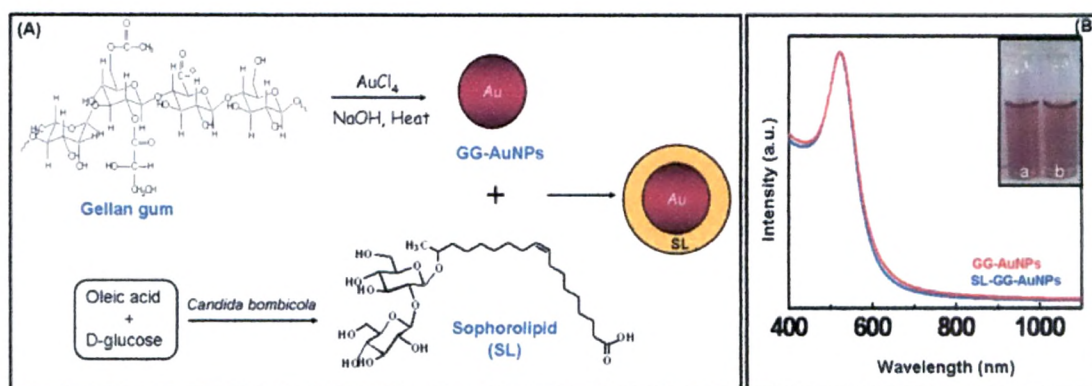
6B.2.5.E MTT assay

After 24 h of incubation, MTT (5 mg/mL, 20 μ L) was added to respective set of cells and the plates were incubated for an additional 4 h. After 4 h of incubation, the medium was removed and 200 μ L DMSO was added to dissolve the formazan crystals resulting from the reduction of the tetrazolium salt only by metabolically active cells. The absorbance of dissolved formazan was measured at 570 nm using microplate reader. Since the absorbance directly correlated with the number of viable cells, the percent viability was calculated from the absorbance.

6B.2.6 Cellular uptake and apoptosis studies using confocal laser scanning microscopy Confocal laser scanning microscopy was used to study the cellular uptake of Texas red labeled SL-AuNPs and PEG-SL-AuNPs and apoptotic activity of DOX-SL- AuNPs and DOX-PEG-SL-AuNPs on various cell lines. The morphology changes of the glioma cells were observed on optical microscopy. After incubation, the cover slips were washed extensively with ice-cold phosphate buffered saline (PBS) and fixed in 4% paraformaldehyde for 10 min at room temperature. After repeated rinses in PBS, cells were blocked in 5% BSA in PBS for 30 min at room temperature. Later the cells were again washed in PBS in dark and then the nucleus was counterstained with 4'-6-Diamidino-2-phenylindole (DAPI) for 10 min and the cells were mounted onto glass slides with 1,4-diazobicyclo-2,2,2-octanex (DABCO) as mounting medium. The cover slips were then observed using confocal microscope. The images were captured by camera coupled with microscope and processed using the computer based programmable image analyzer.

6B.3 Results and discussion

To perk up the function of AuNPs as drug delivery vehicle, we studied the bioconjugation of two different capping agents on GG-AuNPs. In the first approach, sophorolipid was conjugated with GG-AuNPs dispersion (SL-AuNPs) and in the second approach the GG-AuNPs were first conjugated with SL and then conjugated with PEG (PEG-SL-AuNPs). Both conjugations were carried out at room temperature. The UVA/vis spectroscopy of SL-AuNPs and PEG-SL-AuNPs was conferred with that of GG-AuNPs in order to monitor any change in the surface plasmon band after conjugation with SL and PEG-SL [Scheme 6B.1(b)].



Scheme 6B.1: (a) Scheme diagram showing synthesis of gold nanoparticles and sophorolipid conjugated gold nanoparticles and (b) UV/Vis absorption spectra of sophorolipid and Poly (ethylene glycol) conjugated gold nanoparticles.

The AuNPs had a strong absorption peak at 520 nm due to the characteristic surface plasmon resonance. The broadening and red shift of the surface plasmon band is normally associated with the aggregation of the AuNPs consequent to surface modification.^[75] In case of SL-AuNPs, the information drawn from the UV/Vis spectra indicated that the conjugation of SL on GG-AuNPs did not cause any change in the surface plasmon band of AuNPs. The SL conjugated colloidal AuNPs dispersion was highly stable without any aggregation or change in color. Upon addition of PEG to SL-AuNPs dispersion, there was slight change in the absorption spectrum. The decrease in surface plasmon intensity was observed with change in surface plasmon peak to 524 nm compared to 520 nm of GG-AuNPs and SL-AuNPs. Scheme 6B.1(b) shows very minimal broadening of the peak and small shift in the peak position. This was a clear indication that conjugation with SL and PEG did not cause any major change in the characteristic properties of AuNPs.

To demonstrate the versatility of SL-AuNPs and PEG-SL-AuNPs in biomedical application, the dispersion stability of SL-AuNPs and PEG-SL-AuNPs was evaluated by assessing the formation of aggregates and change in the color in the presence of different pH and electrolytic conditions. Detachment of SL or PEG from

AuNPs would cause the nanoparticles to aggregate, which could be monitored by measuring the disappearance of the characteristic plasmon absorption peak and the appearance of a peak between 600 and 700 nm.⁷⁶¹ In case of GG-AuNPs [Figure 5A. 7(a)], after adjusting the pH of the AuNPs dispersion to 2, the AuNPs immediately precipitated out, this was clearly evident by the change in the intensity, position and additional peak at 650 nm. The SL-GG-AuNPs dispersion did not show any discernible change in the position at 520 nm in the pH window of 4-12 [Figure 6B. 11(a,c)]. Only when the pH of SL-GG-AuNPs was adjusted to 2, the dispersion owed some instability but no additional peak was observed.

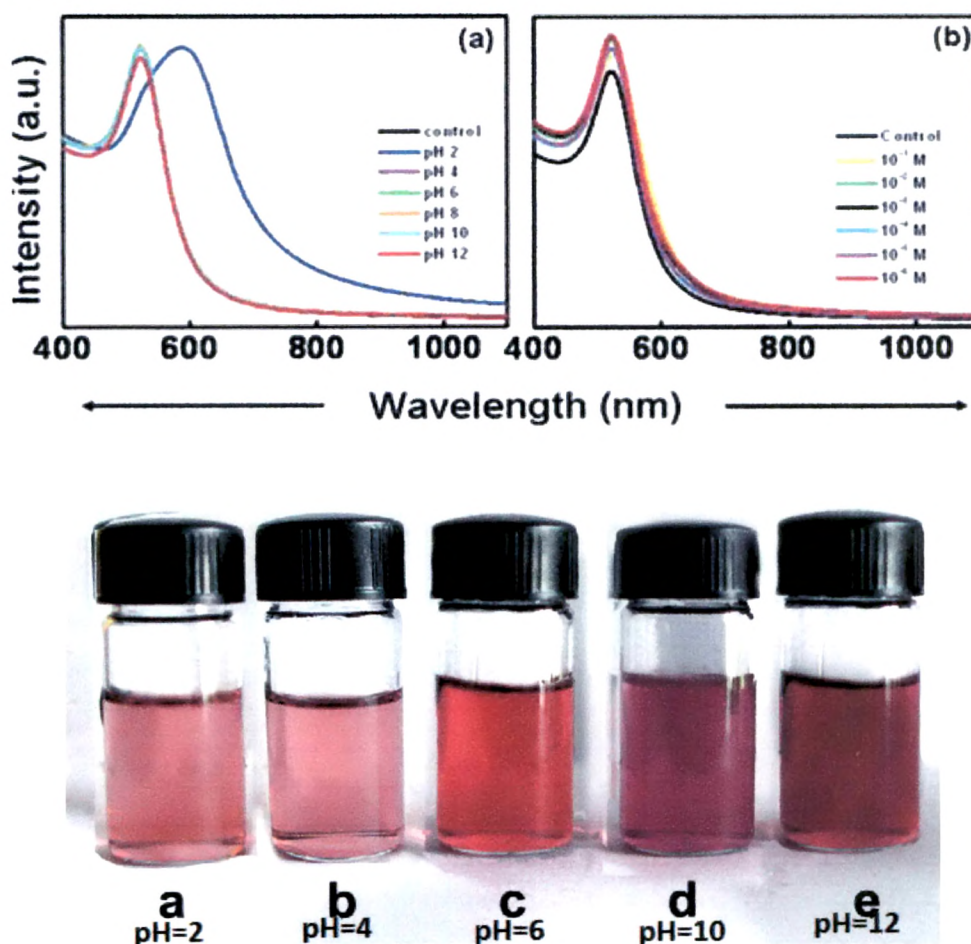


Figure 6B.1: UV/Vis absorption spectra of sophorolipid conjugated gold nanoparticles (a, c) pH study and (b) electrolyte study.

The addition of electrolyte (sodium chloride, 10^{-1} M to 10^{-6} M) also caused no aggregation in the SL-AuNPs [Figure 6B. 1(b)]. The minimal change in the surface plasmon resonance of SL-AuNPs under the above experimental conditions indicated the extra stability imparted to AuNPs due to conjugation with SL. This is in accordance with the recent reports where higher stability to metal nanoparticles in the presence of oleic acid derived SL when used as reducing/capping agent was demonstrated.^[61,62] To confirm the dispersion stability of PEG-SL-AuNPs, nanoparticles were again evaluated under the condition of wide pH range and different electrolyte concentration (Figure 6B. 2).

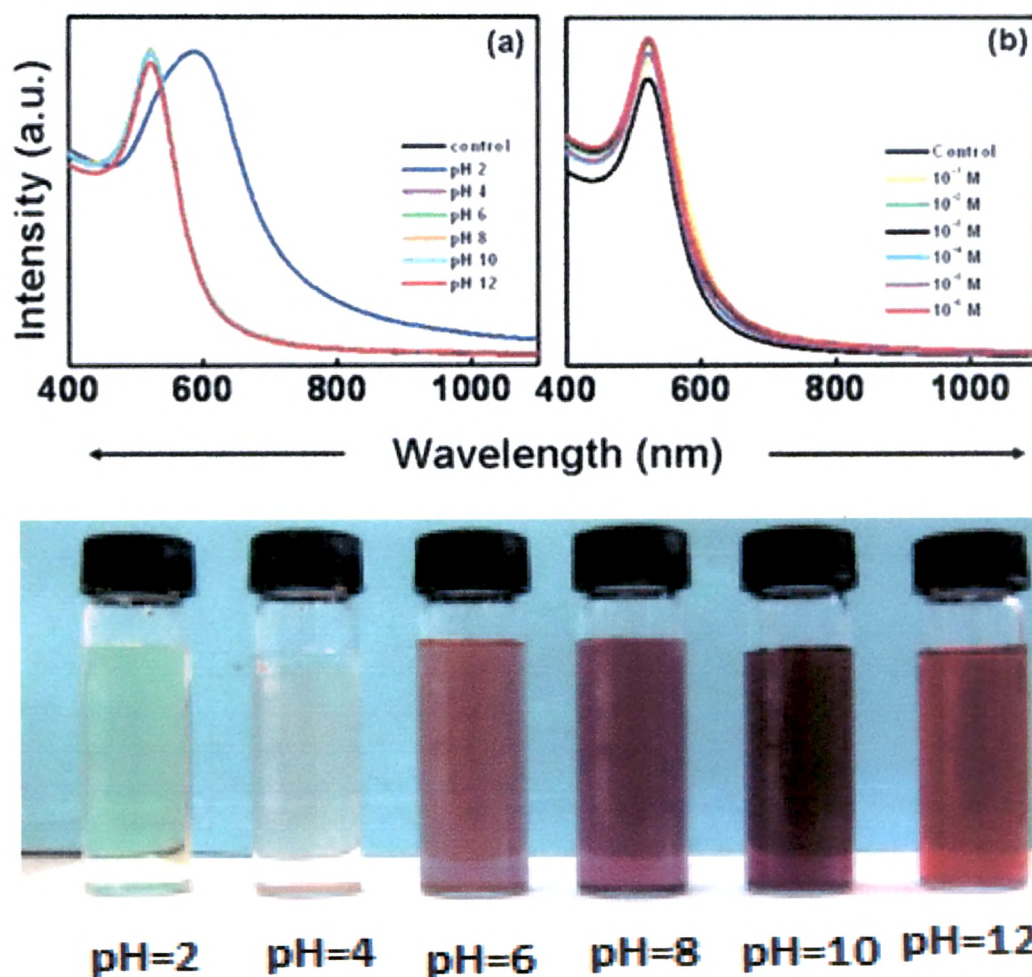


Figure 6B.2: UV/Vis absorption spectra of poly(ethylene glycol)-sophorolipid conjugated gold nanoparticles (a, c) pH study and (b) electrolyte study.

The PEG coating around the AuNPs serves as a protective biological layer to improve particle stability and preventing particle agglomeration.^[77] Figure 6B.2 (a,c) shows that there is no change of the peak position maximum of PEG-SL-AuNPs upon conjugation with AuNPs. Adding HCl or NaOH to an aqueous suspension of the PEG-SL-AuNPs does not affect the UV/Vis spectra (i.e., no particle aggregation) over a pH range of 2-12. Miyamoto et al., synthesized completely dispersible PEG-AuNPs having pH stability between 4-10.^[78] The PEG-SL-AuNPs were then exposed to salt concentrations (10^1M to 10^{-6}M , NaCl). The assembly of a layer of the hydrophilic polymer PEG on the particle surface afforded steric stabilization of AuNPs in salt, thus preventing their aggregation. There was no change in the UV/Vis spectra of PEG-SL-AuNPs monitored upto salt concentration 10^1M , The PEG-SL-AuNPs were stable under wide pH range and various salt concentrations without any aggregation or change in color of the colloidal dispersion. TEM was employed to study the morphology of SL-AuNPs and PEG- SL-AuNPs. Figure 3 and 4 shows the representative TEM images and particles size distribution recorded from SL-AuNPs and PEG-SL-AuNPs respectively.

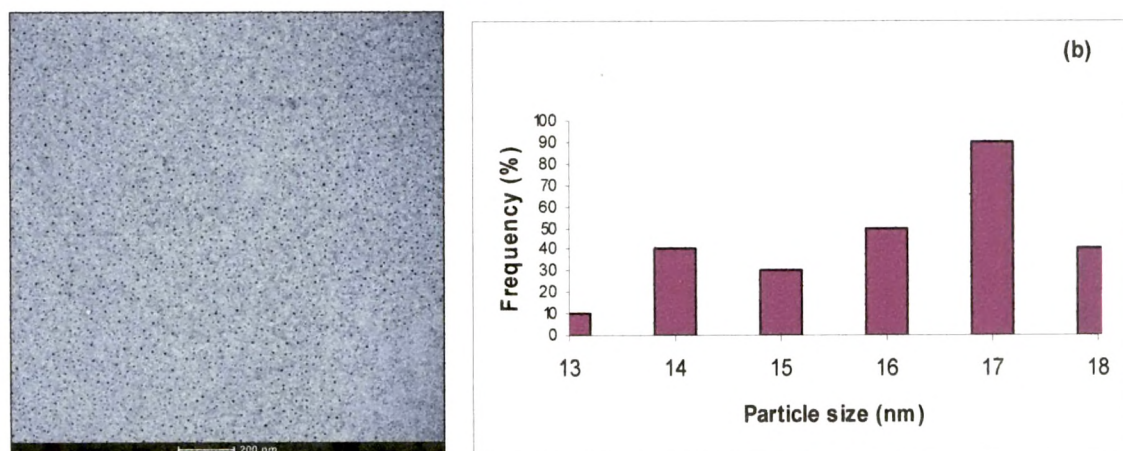


Figure 6B.3: (a) TEM image of sophorolipid conjugated gold nanoparticles and (b) size distribution of the same.

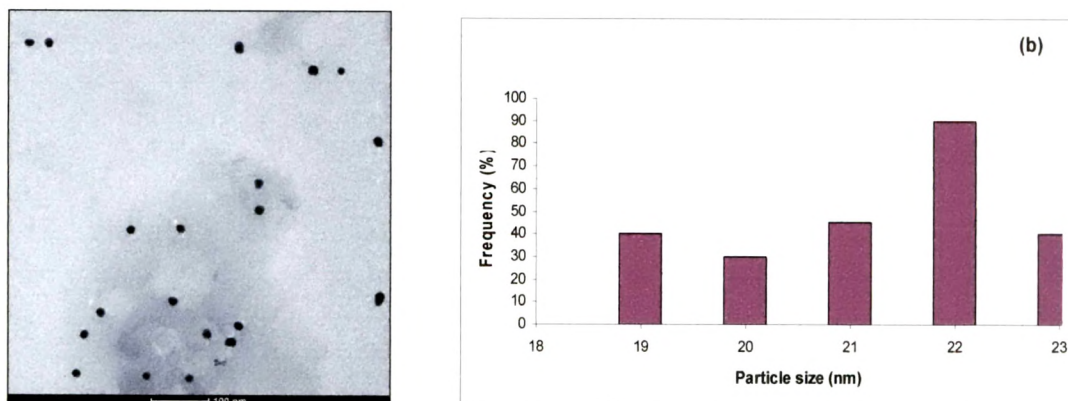


Figure 6B.4: (a) TEM image of poly(ethylene glycol)-sophorolipid conjugated gold particles and (b) particle size distribution of the same.

The SL and PEG-SL conjugated AuNPs images illustrated that upon modification, the average particle size increases to 17 nm and 22 nm respectively. The particle size distribution is shown in figure 6B. 3 and 4(b). The average particle size increased relative to GG-AuNPs (14 nm), due to the conjugation of SL and PEG on AuNPs. The information obtained from TEM concluded that the SL-AuNPs and PEG-SL-AuNPs were uniform in shape, size and free of aggregation and the conjugation of SL and PEG did not affect the overall morphology of the synthesized AuNPs.

At neutral pH, the zeta potential of SL-AuNPs and PEG-SL-AuNPs was -40.64 mV and -38.98 mV respectively. Exposure of AuNPs to SL and PEG indicated that the surface coating was capable of protecting the nanoparticles against aggregation, making them electrostatically stable^[79] and that modified nanoparticles retain their surface charge. These results were in agreement with the results obtained from UV/Vis and TEM analysis. The surface charge and size of the nanoparticles were not significantly affected by surface modification, thus enabling the direct evaluation of the effectiveness of the targeting ligand for activity.^[80]

In order to confer higher stability to SL and PEG conjugated AuNPs, powder form of the nanoparticles was obtained by using spray drying technique. The spray dried SL-AuNPs and PEG-SL-AuNPs thus obtained were ruby red colored free flowing powder [Figure 6B. 5 and 6 (a)]. The resultant redispersed nanoparticles exhibited identical absorption spectra to that of AuNPs before spray drying [Figure 6B. 5 and 6 (b)]. There was neither peak shift nor any additional peak observed in the UV/Vis spectra of SL-AuNPs and PEG-SL-AuNPs, which confirmed that the spray drying had no effect on characteristic properties of SL and PEG conjugated AuNPs. The TEM images of spray dried SL-AuNPs and PEG-SL-AuNPs

are shown in figure 6B.7. The spray dried nanoparticles were spherical in shape and well dispersed. The spray drying did not affect the overall assembly of the nanoparticles. The average particle size of the redispersed AuNPs was same in comparison to the nanoparticles before spray drying [Figure 6B (3 and 4)]. The TEM images were in agreement to the UV/Vis spectra of the SL and PEG conjugated AuNPs that the spray drying formed nanoparticles were uniform in shape, size and free of aggregation.

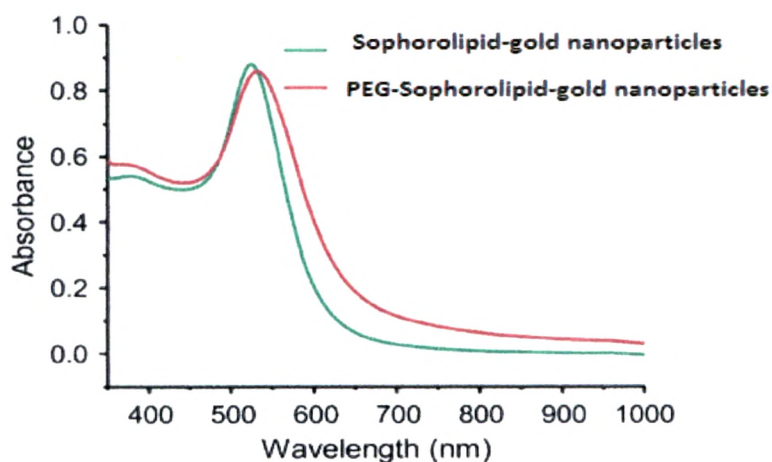


Figure 6B.5: (a) Spray dried powder of sophorolipid and redispersed gold particles. (b) UV/Vis absorption spectra of spray dried sophorolipid conjugated gold nanoparticles.

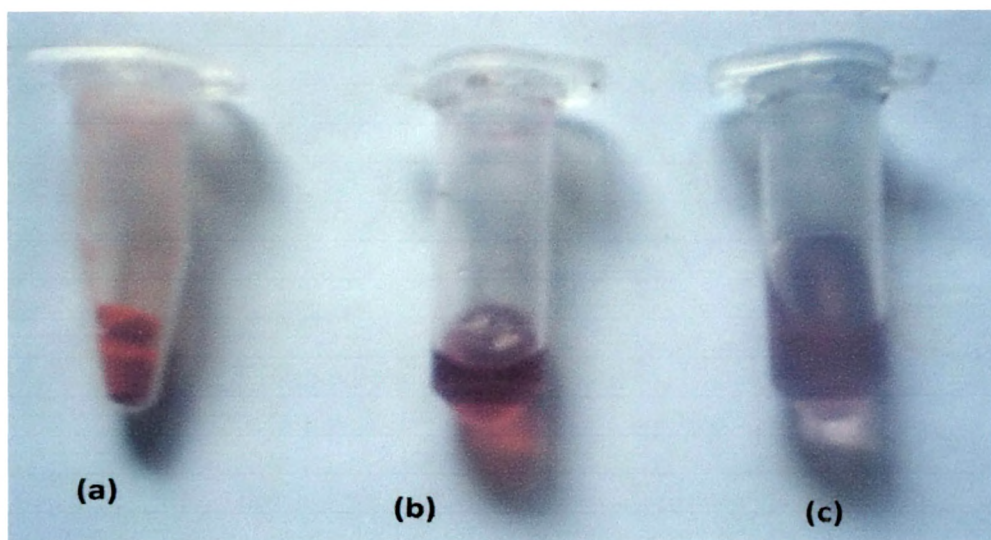


Figure 6B.6: (a) Spray dried powder of poly(ethylene glycol)-sophorolipid and redispersed gold nanoparticles. (b) UV/Vis absorption spectra of spray dried poly(ethylene glycol)-sophorolipid conjugated gold nanoparticles.

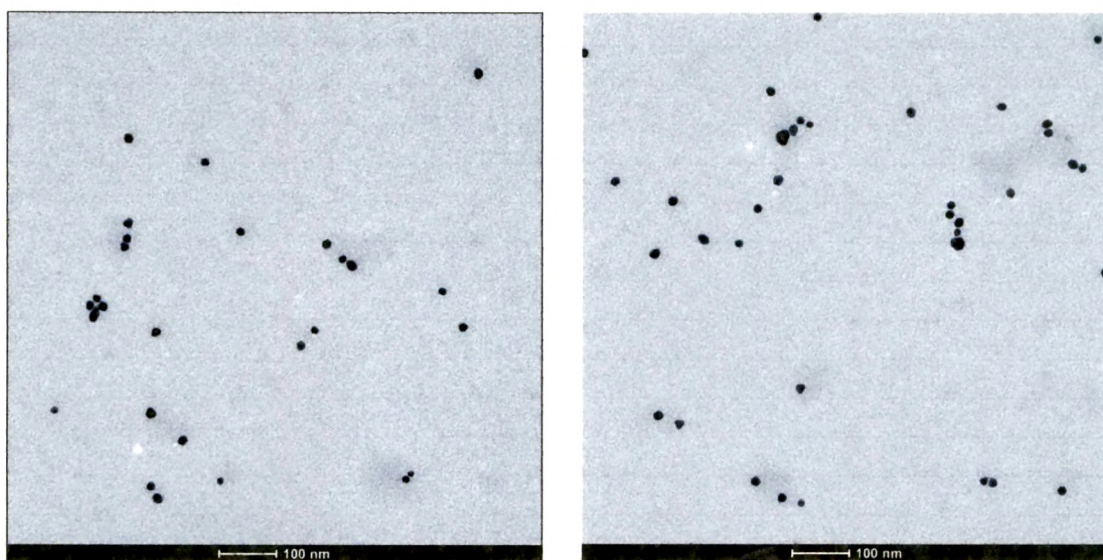


Figure 6B.7: TEM images of spray dried (a) sophorolipid and (b) poly(ethylene glycol)-sophorolipid conjugated gold nanoparticles.

The spray dried SL-AuNPs and PEG-SL-AuNPs were also monitored for long term stability under temperature condition of 25°C/65% RH (room temperature). The spray dried SL-AuNPs and PEG-SL-AuNPs were stable during the storage period of 6 months [Figure 6B. 8 (a,b)]. It was observed that the surface plasmon peak intensity of SL-AuNPs decreased after 3 months of storage may be due to slight aggregation of the nanoparticles during the stability period but there no change in the peak position and no additional peak were observed.

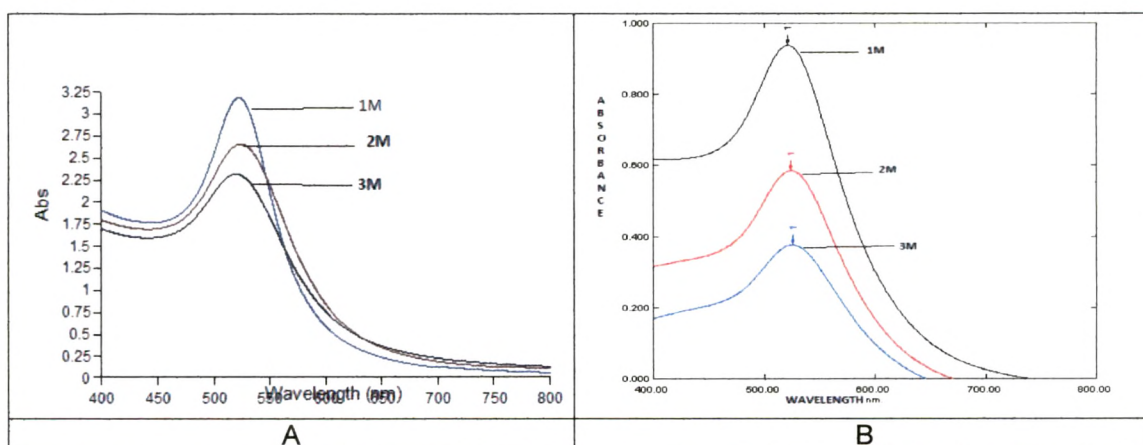


Figure 6B.8: Stability study of spray dried, t-6 months (a) sophorolipid and (b) poly(ethylene glycol) sophorolipid conjugated gold nanoparticles.

In case of PEG-SL-AuNPs, there was no change in the surface plasmon peak position during the study period of 6 months. The SL-AuNPs and PEG-SL-AuNPs had definitely attained more stability than the unconjugated GG-AuNPs. It is remarkable that the AuNPs remain stable during the solid state and reconstituted easily in aqueous media without the loss of their nanoparticulate properties. The long term stability could be attributed to the high stability properties of SL and PEG. The SL-AuNPs and PEG-SL-AuNPs dispersion can be easily stored as powdered form without compromising the stability as well as properties of the nanoparticles and can be redispersed whenever required. The highest colloidal stability and excellent redispersibility even after spray drying of SL and PEG conjugated AuNPs could be of great importance for their practical biomedical use.

To understand the cellular uptake of SL-AuNPs and PEG-SL-AuNPs, fluorescent marker Texas red was conjugated with nanoparticles. The amount of Texas red conjugated to SL-AuNPs and PEG-SL-AuNPs was calculated to be 0.99 ng/ μ L and 1.26 ng/ μ L respectively. The zeta potential of SL-AuNPs reduced from -40.6 mV to -24.1 mV and PEG-SL-AuNPs reduced from -34.98 mV to -15.134 mV upon Texas red loading. The decrease in the zeta potential can be taken as an indication of Texas red conjugation to SL-AuNPs and PEG-SL-AuNPs. After conjugation, the cellular uptake of labeled SL-AuNPs and PEG-SL-AuNPs was studied on human glioma cell line LN-229. The untreated cells were taken as control for the experiment. Cellular uptake using confocal microscopy (Figure 9 and 10) showed that the nanoparticles were efficiently internalized in tumor cells within 3 h of incubation. Gold nanoparticles were clearly observed inside the cells as red dots [Figure 6B, 9, 10 (c)]. The cellular uptake of SL-AuNPs and PEG-SL-AuNPs was observed similar to the GG-AuNPs. The nanoparticles were localized mainly in the cytoplasm and perinuclear region of the cells. Reports on cellular uptake of PEG coated AuNPs have indicated that if the internalization in cells is through endocytotic process, nanoparticles tend to converge to the perinuclear area.^[66]

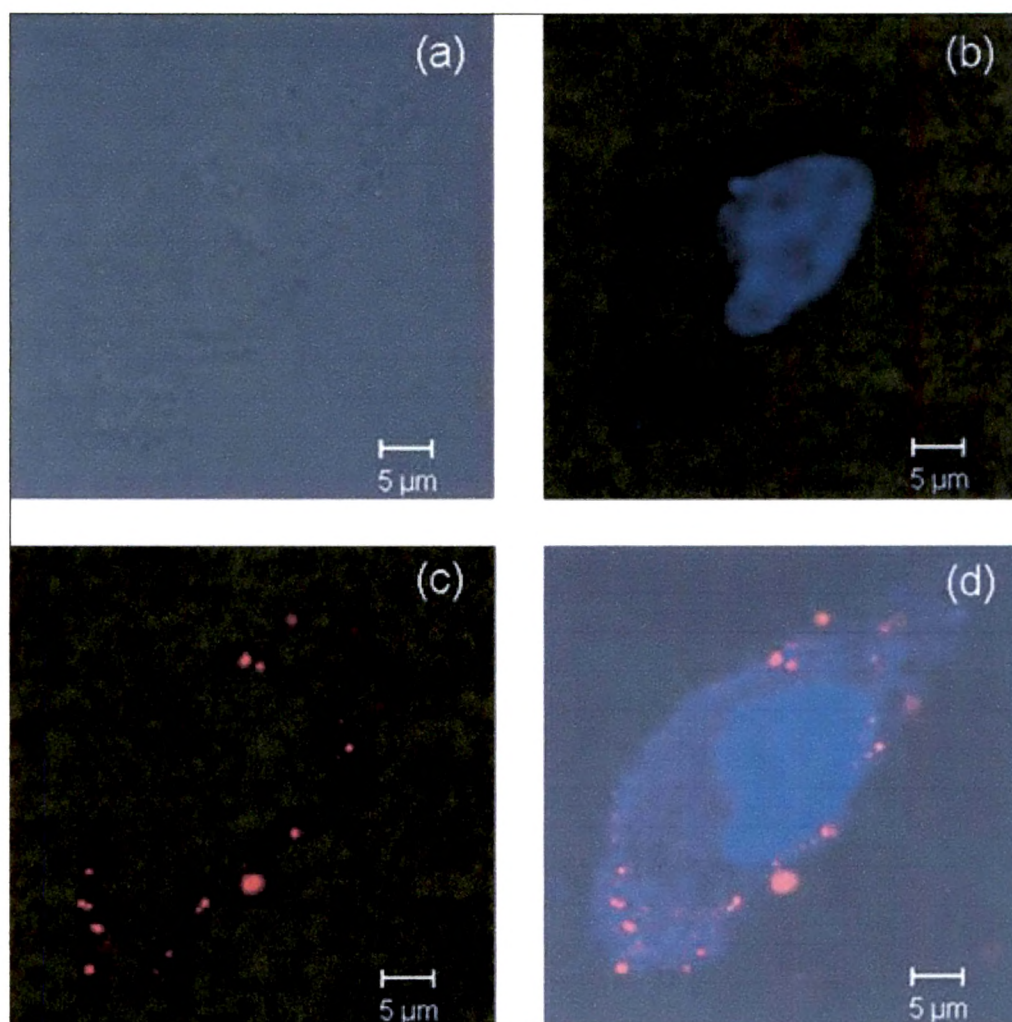


Figure 6B.9: Confocal images of cellular uptake of sophorolipid conjugated gold nanoparticles in human glioma cell lines LN-229. (a) Phase (b) DAPI (c) gold nanoparticles and (d) overlaid (b&c).

Figure 6B.10: Confocal images of cellular uptake of poly(ethylene glycol)-sophorolipid conjugated gold nanoparticles in human glioma cell lines LN-229. (a) Phase (b) DAPI (c) gold nanoparticles and (d) overlaid (b&c).

After characterizing the SL-AuNPs and PEG-SL-AuNPs, DOX was loaded onto AuNPs. Based on the UV/Vis absorbance studies, the loading efficiency of DOX on SL-AuNPs and PEG-SL-AuNPs was determined to be 85% and 92% respectively. This was found to be higher than the DOX loading observed on GG-AuNPs (75%). The positively charged DOX molecules were bound to the negatively charged SL- AuNPs and PEG-SL-AuNPs surface by electrostatic forces. The increased loading of DOX on SL-AuNPs and PEG-SL-AuNPs was also confirmed by zeta potential. The zeta potential of DOX loaded SL-AuNPs and PEG-SL-AuNPs was measured to be -26.73 mV and -23.50 mV respectively. The decrease in the zeta potential was ascribed to the presence of positively charged DOX molecules on the nanoparticles. Park et al., studied the loading of DOX on porous silicon nanoparticles and reported that the loading of DOX on nanoparticles was by electrostatic forces and that there was a decrease in the zeta potential of the DOX loaded nanoparticles (-32.00 mV) as compared to the blank silicon nanoparticles (- 52.00 mV).^[31] It was clear that even after DOX loading, SL-AuNPs and PEG-SL- AuNPs remained in suspension by their electrostatic repulsion and maintained the negative charge on the surface.

The TEM images recorded from the DOX loaded SL-AuNPs and DOX loaded PEG- SL-AuNPs [Figure 6B. 11] indicated that the overall structure of the nanoparticles and their assemblies were not different in comparison to blank SL-AuNPs and PEG- SL-AuNPs. The TEM images of DOX loaded AuNPs retain their morphology after conjugation giving credence to the assertion that DOX loading neither causes much change in their size or nor lead to any aggregation. The particle size distribution of DOX-AuNPs also revealed that the average particle size did not change as there was no significant change in the particle size before and after loading of DOX on SL-AuNPs and PEG-SL-AuNPs.

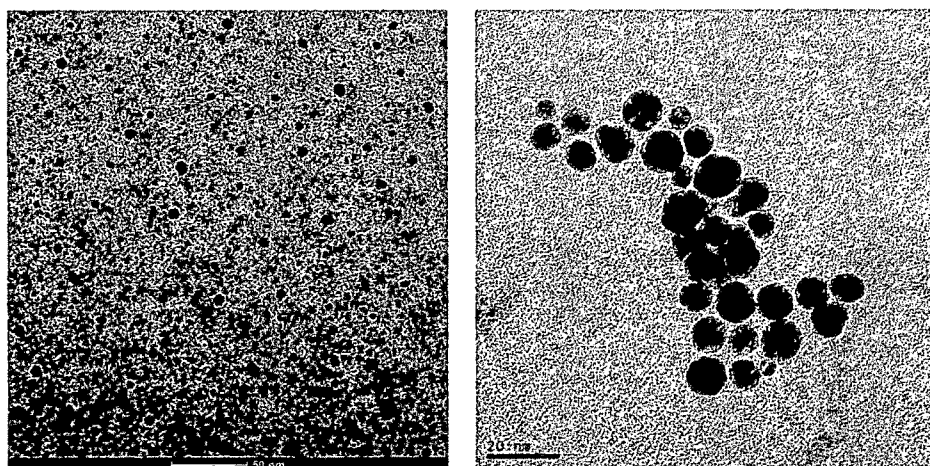


Figure 6B.11: TEM images of doxorubicin loaded (a) sophorolipid and (b) poly (ethylene glycol)-sophorolipid conjugated gold nanoparticles.

The binding and stability of DOX molecule after loading-on SL-AuNPs and PEG-SL-AuNPs was studied using fluorescence spectroscopy. Doxorubicin hydrochloride exhibits a unique fluorescence emission spectrum that is susceptible to changes in its microenvironment.^[36] The emission spectra of DOX solution and DOX loaded on SL-AuNPs and PEG-SL-AuNPs was recorded from 490 to 800 nm at a fixed excitation of 480 nm. The fluorescence emission spectra recorded are shown in figure 6B. 12. There was no major change in the emission profile from DOX in DOX loaded SL-AuNPs and PEG-SL-AuNPs and the peaks at 597 nm and 635 nm as observed in pure DOX were retained. After binding of DOX molecules to AuNPs, the fluorescence intensity was reduced and this quenching of intensity could be attributed to the electrostatic or hydrogen bond formation between the DOX molecule and AuNPs. The preservation of the fluorescence signature supports the claim that DOX structure was retained following complexation with nanoparticles.^[37] The stability of spray dried DOX loaded SL-AuNPs and PEG-SL-AuNPs were monitored over a period of three months using fluorescence spectroscopy (Figure 6B.13). It was found that the spray dried DOX loaded SL-AuNPs and PEG-SL- AuNPs were stable during its storage period of 3 months. There was no change in the fluorescence spectra profile of DOX loaded SL or PEG conjugated AuNPs.

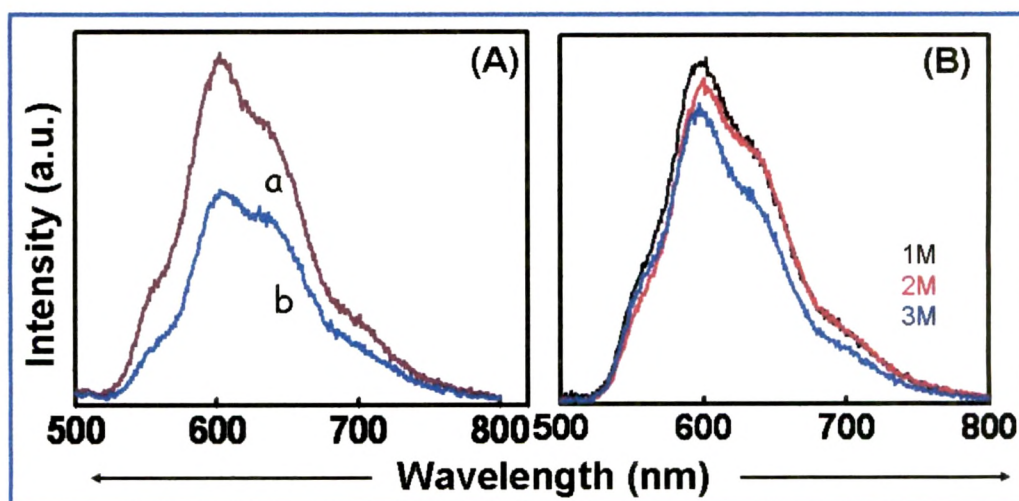
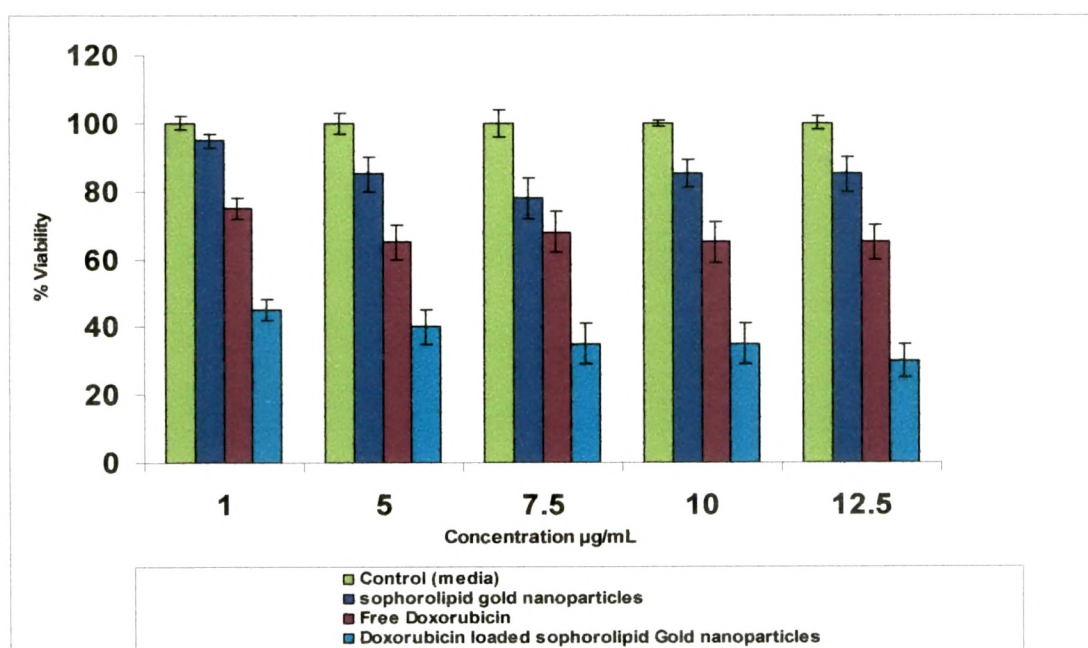


Figure 6B.12: Fluorescence spectra of doxorubicin (A) Sophorolipid (B) poly(ethylene glycol)-sophorolipid conjugated gold nanoparticles. (a) doxorubicin solution and (b) doxorubicin loaded gold nanoparticles.

Figure 6B.13: Stability study of spray dried doxorubicin loaded, $t=3$ months (a) sophorolipid and (b) poly(ethylene glycol)-sophorolipid conjugated gold nanoparticles.

After successful synthesis and characterization of SL-AuNPs, PEG-SL-AuNPs and DOX loaded SL and PEG-SL conjugated AuNPs, *in vitro* cytotoxicity of different formulations namely SL-AuNPs, PEG-SL-AuNPs, DOX-SL-AuNPs, DOX-PEG-SL- AuNPs, free DOX solution and only culture and media was evaluated using MTT assay against human glioma cell line LN-229 and human glioma stem cell line HNGC-2. The well that received only culture media was regarded as control with a cell viability of 100%. Figure 6B.14 shows the percent viability of LN-229 cell line after exposure to SL-AuNPs and DOX, in pure solution form and as loaded on SL-AuNPs for 24 and 48 h respectively. In case of SL-AuNPs, at highest concentration 12.5 $\mu\text{g/mL}$, the cell viability was 80% in 24 h and reached 50% in 48 h.

(a)



(b)

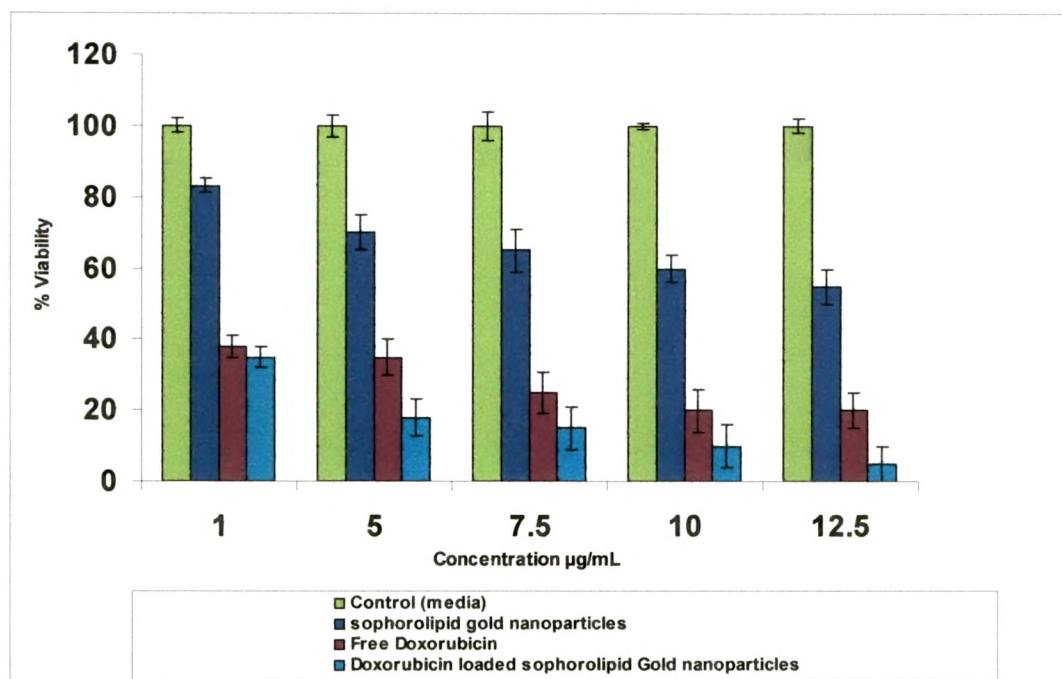
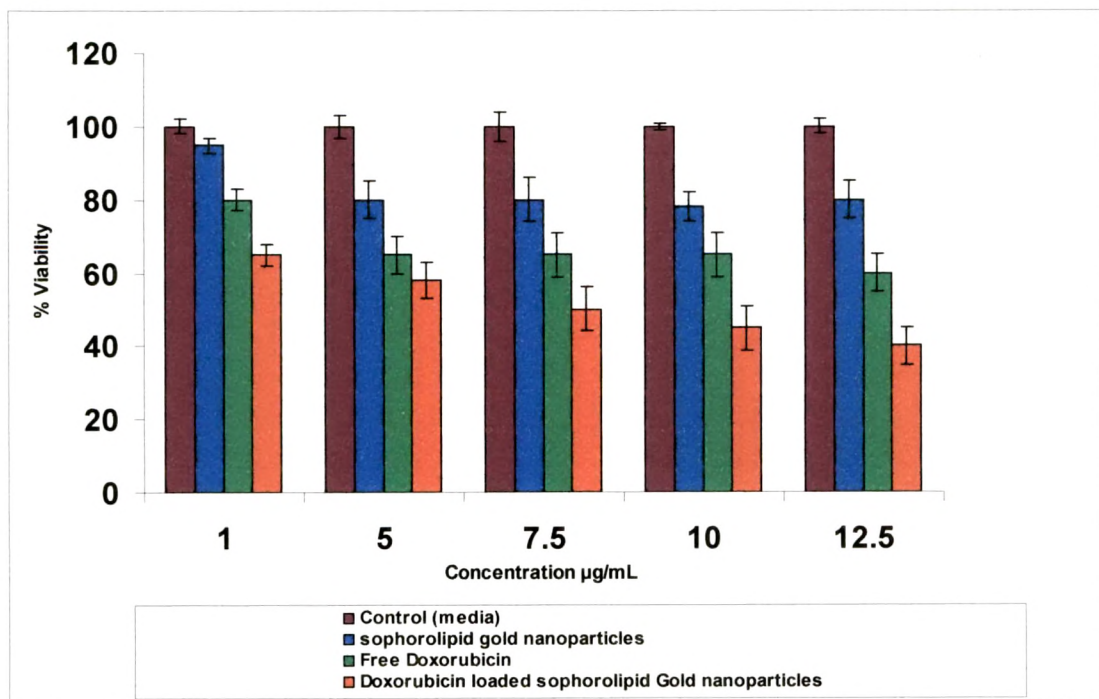


Figure 6B.14: Viability of LN-229 after (a) 24 and (b) 48 h, after exposure to (from left to right): control (media), sophorolipid gold nanoparticles, doxorubicin solution and doxorubicin loaded sophorolipid gold nanoparticles.

It was apparent that the LN-229 cells when incubated with SL-AuNPs had lower viability than the blank GG-AuNPs [Figure 6A. 7 and 8]. As SL exhibit anticancer properties, it can effectively decrease the viability when used against various cancer cells lines.^[59,81] We extended our studies on these cell lines with DOX loaded SL-AuNPs. At the end of 24 h incubation, the DOX loaded SL-AuNPs effectively decreased the viability to 27% (at concentration of 12.5 µg/mL) as compared to 59% as found in case of free DOX solution [Figure 6B. 14(a)], By the end of 48 h of incubation, the viability of LN-229 cell with DOX loaded SL-AuNPs reached 2% compared to 16% of free DOX solution [Figure 6B. 14(b)]. Further, results of these studies illustrate that the presence of SL functionalized AuNPs apparently inhibits the growth of human glioma stem cells. The most appealing result were that upon 48 h exposure to SL-AuNPs [Figure 6B. 15(b)], human glioma stem cells HNGC-2 also showed similarly cell viability of 54% at concentration of 12.5 pg/mL similar to LN-229 cell line. This clearly establishes that conjugation with sophorolipid alone on the nanoparticles surface leads to cytotoxicity towards not just cancerous cells but towards stem cells also. After 24 h of exposure, in case of free DOX solution and DOX loaded SL-AuNPs, the cell viability within the checked concentration range (1.0µg/mL to 12.5 pg/mL)

was 79.55% to 59.07% for free DOX and 60.99% to 40.01% for DOX loaded SL-AuNPs [Figure 6B. 15(a)], After 48 h of incubation [Figure 6B. 15(b)], the DOX loaded SL-AuNPs exhibited more cytotoxicity against human glioma stem cells as compared to free DOX solution. Here, the maximum cell viability achieved via 12.5 (mg/mL at the end of 48 h was 32.34% for free DOX solution and 8.88% for DOX loaded SL-AuNPs. Thus, the DOX loaded SL-AuNPs were able to significantly decrease the cell viability indicating that the combination therapy have potential in eradication of glioma cancer cells and even glioma stem cells. Liu et al., studied the combination therapy using stealthy liposomal vinorelbine plus stealthy liposomal parthenolide and reported that combination therapy may be helpful to provide a potential strategy for eradication of cancers by targeting both cancer and cancer stem cells together.^[82]

(a)



(b)

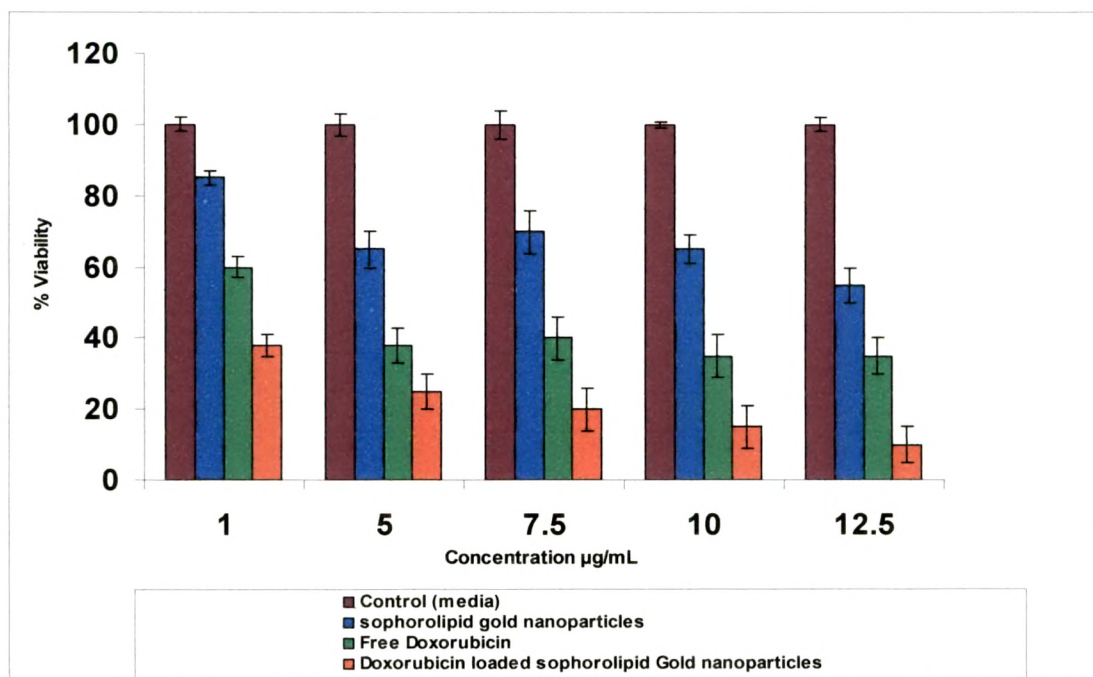
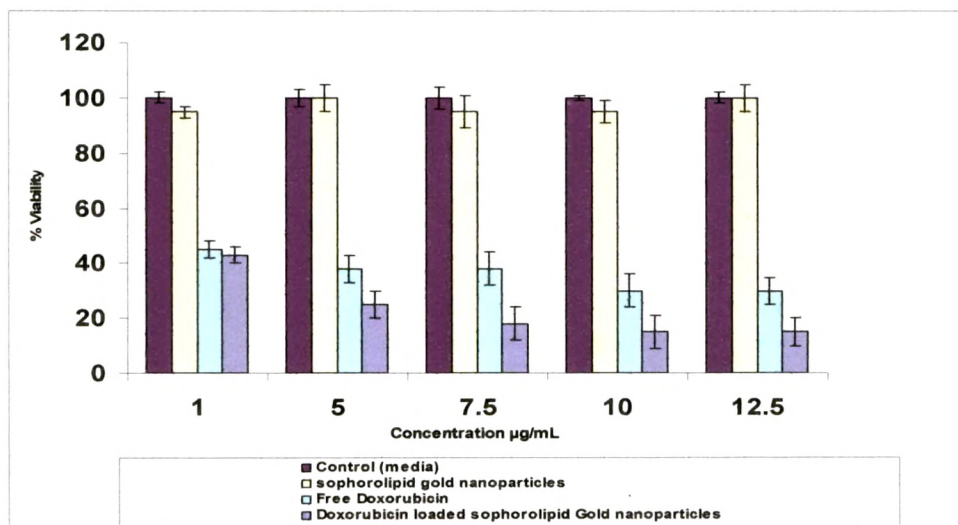


Figure 6B.15: Viability of HNGC-2 after (a) 24 and (b) 48 h, after exposure to (from left to right): control (media), sophorolipid gold nanoparticles, doxorubicin solution and doxorubicin loaded sophorolipid gold nanoparticles.

The surface modified PEG are studied for its use in diagnostic and therapeutic, as it readily get linked to AuNPs and successively allows attachment of the targeting agents and biomolecules which masks AuNPs from the intravascular immune system and help targeting cancer cells due to the EPR effect. We conjugated PEG with SL-AuNPs and studied its cytotoxic effects against human glioma cell line LN- and human glioma stem cell line HNGC-2. The wells that received only culture media were regarded as a control with a cell viability of 100%.

(a)



(b)

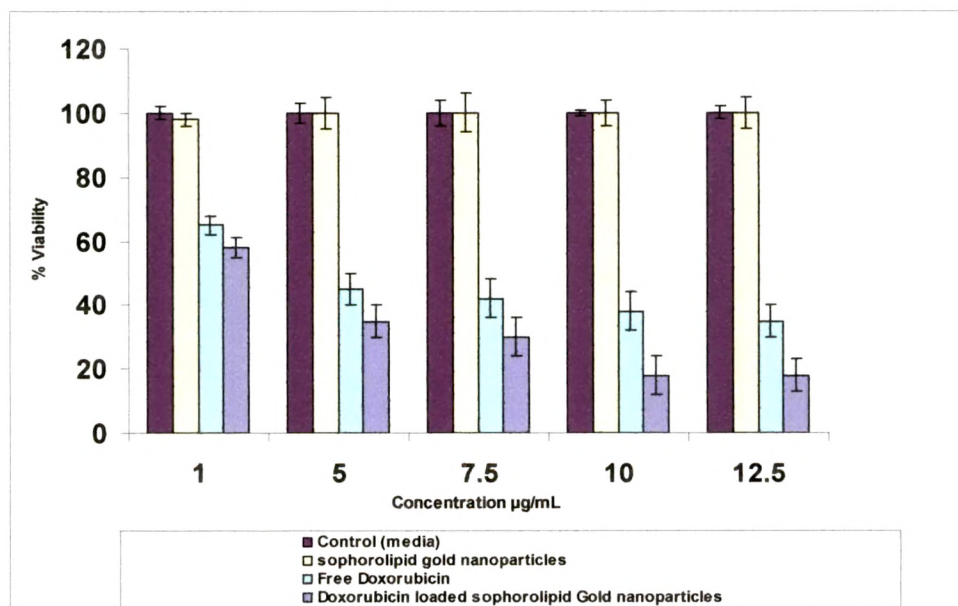


Figure 6B.16: Viability of (a) LN-229 and (b) HNGC-2, after 48 h exposure to (from left to right): control (media), poly(ethylene glycol)-sophorolipid gold nanoparticles, doxorubicin solution and doxorubicin loaded poly(ethylene glycol)-sophorolipid gold nanoparticles.

Shows the percent viability of LN-229 and HNGC-2 cell line to DOX, in pure solution form and as loaded on AuNPs after 48 h respectively. The PEG-SL- AuNPs did not show any cytotoxicity against both glioma cell lines. The conjugation of PEG shielded SL and formed a layer around AuNPs thus making them biocompatible as seen in figure 6B.16 (a & b). In case of human glioma cell line LN- 229, after 48 h of incubation, DOX loaded PEG-SL- AuNPs were able to decrease the cell viability to 9% as compared to 25% for free DOX solution. In case of human glioma stem cell line HNGC-2 [Figure 6B. 16(b)], free DOX solution and DOX loaded PEG-SL-AuNPs gradually increase their cytotoxicity with increasing concentration and the cytotoxicity was dominated by DOX loaded PEG-SL- AuNPs. At the end of 48 h incubation, the cell viability via free DOX solution at the concentration range studied (1.0 µg/mL to 12.5 µg/mL) was from 62-28% and for DOX loaded nanoparticles, the decrease was from 53-15%.

The rationale behind this could be the better cell penetration of the DOX loaded functionalized nanoparticles conjugate as compared to free DOX alone.^[83] This may trigger a rapid release of DOX from the DOX conjugated AuNPs after they internalized into the tumor cells, thereby greatly enhancing the cell cytotoxicity.^[84] Thus it is apparent that DOX could move into the drug resistant cancer cells more easily in the presence of AuNPs than that with DOX alone.

The phase contrast images were taken to see the morphological changes due to effect of various treatments on the different cell lines. The morphology of the control (cells in media) of LN-229 and HNGC-2 was not affected and were highly proliferated [Figure 6B.17&18 (a)]. In case of the SL conjugated AuNPs (LN-229 and HNGC-2), the morphology of the blank SL-AuNPs treated cells also changed. The cells were circular and the cells were detached from the surface [Figure 6B. 17(b)]. These results were in agreement to the cytotoxicity assay. The SL-AuNPs itself was able to decrease the cell proliferation and change the morphology of cells. The effect of DOX on the cancer cells was also very clear. The morphology and number of cells were changed in comparison to the control and most of the cells were detached from the surface and were circular in shape. In case of PEG-SL- AuNPs, the images clearly demonstrated the wrapping of PEG around the AuNPs to remain biocompatible, hence no effect on the cells to proliferation.

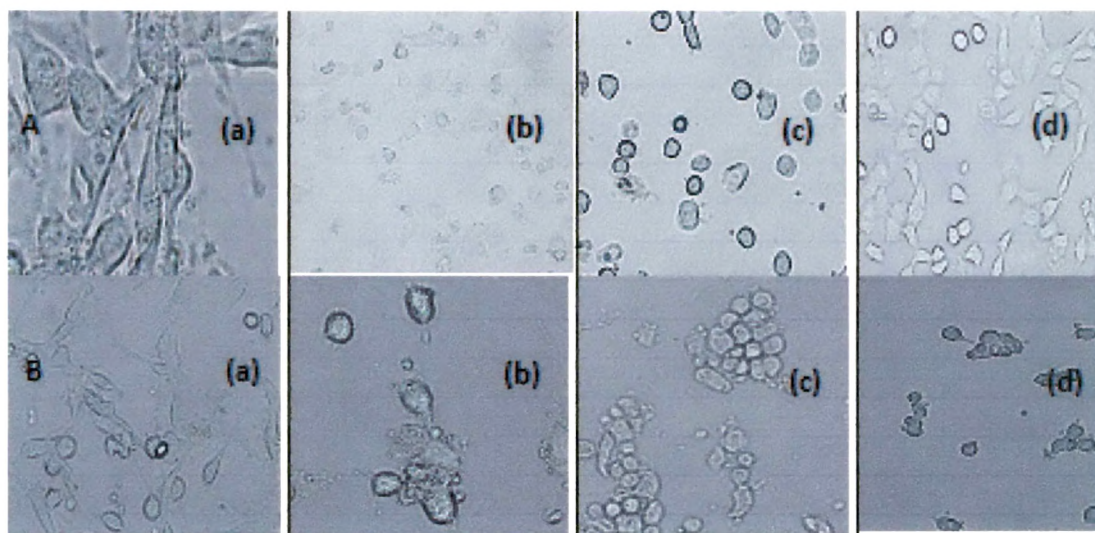


Figure 6B.17: Phase contrast images to demonstrate the morphology changes on (A) human glioma cell line LN-229 (B) human glioma stem cell line HNGC-2 due to (a) media (b) sophorolipid nanoparticles (c) free doxorubicin solution (d) doxorubicin loaded sophorolipid conjugated gold nanoparticles.

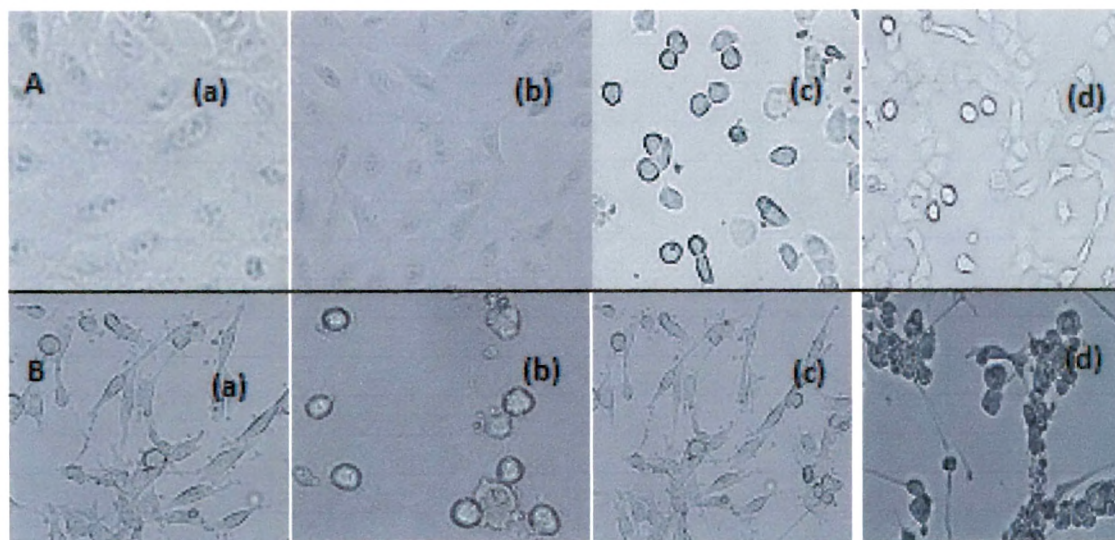


Figure 6B.18: Phase contrast images to demonstrate the morphology changes on (A) human glioma cell line LN-229 (B) human glioma stem cell line HNGC-2 due to (a) media (b) poly(ethylene glycol)-sophorolipid nanoparticles (c) free doxorubicin in (d) doxorubicin loaded poly(ethylene glycol)-sophorolipid conjugated gold nanoparticles.

There was no change in the morphology of the blank PEG-SL-AuNPs treated cells [Figure 6B. 18 (b)]. The free DOX and DOX loaded PEG-SL-AuNPs treated cells were highly affected as the number of the cells was very less cells compared to the control and the effect of DOX loaded PEG-SL-AuNPs was more prominent compared to free DOX treated cells [Figure 6B. 18 (c&d)]. The better internalization of AuNPs with DOX was clearly established from confocal studies.

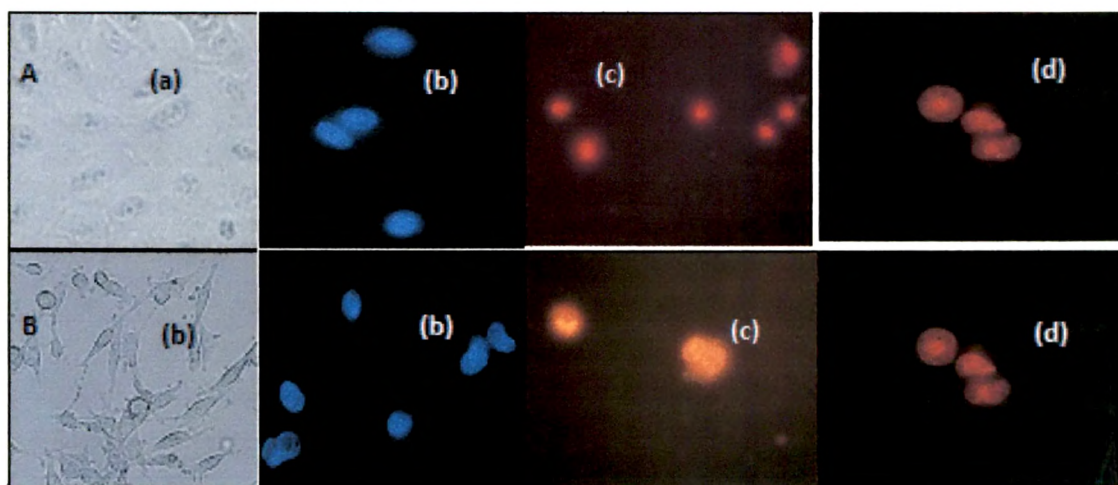


Figure 6B.19: Confocal microscopy images to demonstrate the apoptosis induced by doxorubicin loaded sophorolipid conjugated gold nanoparticles on (A) human glioma cell line LN-229 (B) human glioma stem cell line HNGC-2. (a) Phase (b) DAPI (c) doxorubicin loaded gold nanoparticles and (d) overlaid.

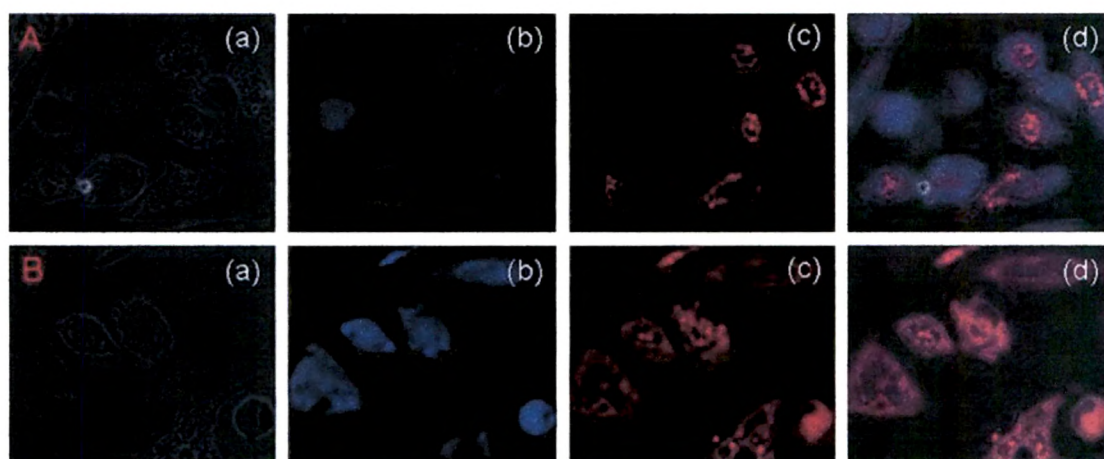


Figure 6B.20: Confocal microscopy images to demonstrate the apoptosis induced by doxorubicin loaded poly(ethylene glycol) -sophorolipid conjugated gold nanoparticles on (A) human glioma cell line LN-229 (B) human glioma stem cell line HNGC-2. (a) Phase (b) DAPI (c) doxorubicin loaded gold nanoparticles and (d) overlaid.

The apoptosis induced by DOX-loaded sophorolipid and polyethylene glycol)- sophorolipid conjugated gold, nanoparticles was evaluated on LN-229 and HNGC-2 cells by confocal microscope. Reports have identified apoptosis as a major mechanism of cell death in exposure to doxorubicin hydrochloride.^[44] During apoptosis or programmed cell death, cells undergo an energy dependent sequence of events, ultimately fragmenting nuclei and cytoplasmic organelles into small membrane sealed apoptotic bodies. Morphologically, rapid cell shrinkage, increase of cell granularity and chromatin condensation are the most obvious changes associated with apoptosis. The apoptosis of DOX loaded AuNPs are shown in figure 6B. 19 & 20. The apoptosis induced by DOX-AuNPs was clearly visible as the cells shrunk to spherical shape. The cytoplasm of the cell was disturbed badly and formed the apoptotic bodies. Because of apoptosis, most of the cells were detached from the cover slips and washing further removed the apoptotic cells but the main apoptosis features like cell shrinkage, chromatin condensation and nuclei fragmentation were clearly observed with the help of confocal microscopy. Confocal images clearly demonstrated the apoptosis induced cell death by DOX loaded AuNPs on human glioma cell lines LN-229 and human glioma stem cell lines HNGC-2.

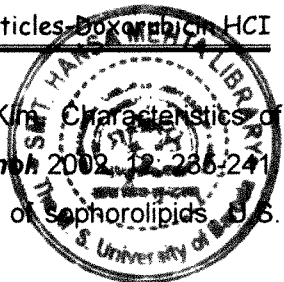
References:

1. A.D. Marco, M. Gaetani, B. Scarpinato. Adriamycin: A new antibiotic with antitumor activity. **Cancer Chemother.** 1969, 53; 33-37.
2. R.S. Benjamin, C.E. Riggs, N.R. Bachur. Pharmacokinetics and metabolism of doxorubicin in man. **Clin. Pharmacol. Ther.**, 1973, 14; 592-600.
3. I.Muller, D. Niethammer, G. Bruchelt. Anthracycline derived chemotherapeutics in apoptosis and free radical cytotoxicity. **Int. J. Mol. Med.**, 1998, 1; 491-504.
4. P. Hau, K. Fabel, U. Baumgart, P. Rummele, O. Grauer, A. Bock, C. Dietmaier, W. Dietmaier, J. Dietrich, C. Dudel, F. Hubner, T. Jauch, E. Drechsel, I. Kleiter, C. Wismeth, A. Zellner, A. Brawanski, A. Steinbrecher, J. Marienhagen, U. Bogdahn. Pegylated liposomal doxorubicin efficacy in patients with recurrent high grade glioma. **Cancer** 2004, 100; 1199-1207.
5. G. Minotti, P. Mennae, E. Salvatorelli, G. Cairo, L. Gianni. Anthracyclines: Molecular advances and pharmacologic developments in antitumor activity and cardiotoxicity. **Pharmacol. Rev.**, 2004, 56; 185-229.
6. R. E. Gonsette. A comparison of the benefits of mitoxantrone and other recent therapeutic approaches in multiple sclerosis. **Expert Opin. Pharmacother.** 2004, 5; 747-765.
7. E.A. Neuwelt, M. Pagel, P. Barnett, M. Glassberg, E.P. Frenkel. Pharmacology and toxicity of intracarotid doxorubicin administration following osmotic blood brain barrier modification. **Cancer Res.**, 1981, 41; 4466-4470.
8. G. Batist, G. Ramakrishnan, C.S. Rao, A. Chandrasekharan, J. Gutheil, T. Guthrie, P. Shah, A. Khojasteh, M.K. Nair, K. Hoelzer, K. Tkaczuk, Y.C. Park, L.W. Lee. Cardiotoxicity and presented antitumour efficacy of liposome encapsulated doxorubicin and cyclophosphamide compared with conventional doxorubicin and cyclophosphamide in a randomized, multicenter trial of metastatic breast cancer. **J. Clin. Oncol.**, 2001, 19; 1444-1454.
9. H. Huang, E. Pierstorff, E. Osawa, D. Ho. Active nanodiamond hydrogels for chemotherapeutic delivery. **Nano Lett.**, 2007, 7; 3305-3314.
10. (a) P. Couvreur, C. Vauthier. Nanotechnology: Intelligent design to treat complex disease. **Pharm. Res.**, 2006, 23; 1417-1450. (b). Y.M. Ning, K. He, R. Dacner R. Sridhara, A. Farrell, R. Justice, R. Padzur. Liposomal doxorubicin in combination with bortezomib for relapsed or refractory multiple myeloma. **Oncology** 2007, 21; 1503-1508.
11. H. Gu, P.L. Ho, E. Tong, L. Wang, B. Xu. Presenting vancomycin on nanoparticles to enhance antimicrobial activities. **Nano Lett**, 2003, 3; 1261- 1263.

12. R. Shukla, V. Bansal, M. Chaudhary, A. Basu, R.R. Bhonde, M. Sastry. Biocompatibility of gold nanoparticles and their endocytotic fate inside the cellular compartment: A microscopic overview. *Langmuir* 2005, 21; 10644- 10654.
13. P.R. Selvakannan, S. Mandal, S. Phadtare, A. Gole, R. Pasricha, S.D. Adyanthaya, M. Sastry. Water dispersible tryptophan protected gold nanoparticles prepared by the spontaneous reduction of aqueous chloroaurate ions by the amino acid. *J. Colloid Interface Sci.*, 2004, 269; 97-102.
14. A. Gole, C. Dash, C. Soman, S.R. Sainkar, M. Rao, M. Sastry. On the preparation, characterization, and enzymatic activity of fungal protease gold colloid bioconjugates. *Bioconjugate Chem.*, 2001, 12; 684-690,
15. A. Gole, C. Dash, V. Ramakrishnan, S.R. Sainkar, A.B. Mandale, M. Rao, M. Sastry. Pepsin gold colloid conjugates: Preparation, characterization, and enzymatic activity. *Langmuir* 2001, 17; 1674-1679.
16. A. Kumar, M. Pattarkine, M. Bhadbhade, A.B. Mandale, K.N. Ganesh, S.S. Datar, C.V. Dharmadhikari, M. Sastry. Pepsin gold colloid conjugates: Preparation, characterization, and enzymatic activity. *Adv. Mater.*, 2001, 13; 341-344.
17. J.D. Gibson, B.P. Khanal, E.R. Zubarev. Paclitaxel functionalized gold nanoparticles. *J.Am. Chem. Soc.*, 2007, 129; 11653-11661.
18. C.D. Medley, J.E. Smith, Z. Tang, Y. Wu, S. Bamrungsap, W. Tan. Pepsin gold colloid conjugates: Preparation, characterization, and enzymatic activity. *Anal. Chem.*, 2008, 80; 1067-1072.
19. V. Kattumuri, K. Katti, S. Bhaskaran, E.J. Boote, S.W. Casteel, G.M. Fent, D.J. Robertson, M. Chandrasekhar, R. Kannan, K.V. Katti. Gum arabic as a phytochemical construct for the stabilization of gold nanoparticles: In vivo pharmacokinetics and X-ray contrast imaging studies. *Small* 2007, 3; 333- 341.
20. J. Roth. Protein glycosylation in the endoplasmic reticulum and the golgi apparatus and cell type-specificity of cell surface glycoconjugate expression: Analysis by the protein a-gold and lectin-gold techniques. *Histochem. Cell Biol.*, 1996, 106; 79-92.
21. L. Olofsson, T. Rindzevicius, I. Pfeiffer, M. Kali, F. Hook. Surface based gold nanoparticle sensor for specific and quantitative DNA hybridization detection *Langmuir* 2003, 19; 10414-10419.
22. V. Selvaraj, M. Alagar, I. Hamerton. Analytical detection and biological assay of antileukemic drug using gold nanoparticles. *Electrochimica Acta* 2006, 52; 1152-1160.
23. G.F. Paciotti, L. Myer, D. Weireich, D. Goia, N. Pavel, R.E. McLaughlin, L. Tamarkin. Colloidal gold: A novel nanoparticle vector for tumor directed drug delivery. *Drug Deliv.*, 2004, 11; 169-183.

24. J.M. Nam, C.S. Thaxton, C.A. Mirkin. Nanoparticle based bio bar codes for the ultrasensitive detection of proteins. *Science* 2003, 301; 1884-1886.
25. X. Huang, P.K. Jain, I.H. El-Sayed, M.A. El-Sayed. Plasmonic photothermal therapy (PPTT) using gold nanoparticles. *Lasers Med. Sci.*, 2008, 23; 217- 228.
26. J. Chen, D. Wang, J. Xi, L. Au, A. Siekkinen, A. Warsen, Z.Y. Li, H. Zhang, Y. Xia, X-Li. Immuno gold nanocages with tailored optical properties for targeted photothermal destruction of cancer cells. *Nano Lett.*, 2007, 7; 1318-1322.
27. H.M. Joshi, D.R. Bhumkar, K. Joshi, V. Pokharkar, M. Sastry. Gold nanoparticles as carriers for efficient transmucosal insulin delivery. *Langmuir* 2006, 22; 300-305.
28. D.R. Bhumkar, H.M. Joshi, M. Sastry, V.B. Pokharkar. Chitosan reduced gold nanoparticles as novel carriers for transmucosal delivery of insulin. *Pharm. Res.*, 2007, 24; 1415-1426.
29. R.T. Tom, V. Suryanarayanan, P.G. Reddy, S. Baskaran, T. Pradeep. Ciprofloxacin protected gold nanoparticles. *Langmuir* 2004, 20; 1909-1914.
30. J.R. Hwu, Y.S. Lin, T. Josephrajan, M.H. Hsu, F.Y. Cheng, C.S. Yeh, W.C. Su, D.B. Shieh. Targeted paclitaxel by conjugation to iron oxide and gold nanoparticles. *J. Am. Chem. Soc.*, 2009, 131; 66-68.
31. J.H. Park, L. Gu, G.V. Maltzahn, E. Ruoslahti, S.N. Bhatia, M.J. Sailor. Biodegradable luminescent porous silicon nanoparticles for in vivo applications. *Nat. Mater.*, 2009, 8; 331-336.
32. T. Mosmann. Rapid colorimetric assay for cellular growth and survival: Application to proliferation and cytotoxicity assay. *J. Immunol. Methods.*, 1983, 65; 55-63.
33. E. Boisselier, D. Astruc. Gold nanoparticles in nanomedicine: Preparations, imaging, diagnostics, therapies and toxicity. *Chem. Soc. Rev.*, 2009, 38; 1759-1782.
34. D.R. Kalaria, G. Sharma, V. Beniwal, M.N.V. Ravi Kumar. Design of biodegradable nanoparticles for oral delivery of doxorubicin: In vivo pharmacokinetics and toxicity studies in rats. *Pharm. Res.*, 2009, 26; 492- 510.
35. P.V. Kamat, S. Barazzouk, S. Hotchandani. Electrochemical modulation of fluorophore emission on a nanostructured gold film. *Angew. Chem. Int. Ed.*, 2002, 41; 2764-2767.
36. N. Husain, R.A. Agbaria, I.M. Warner. Spectroscopic analysis of the binding of doxorubicin to human alpha-1 acid glycoprotein. *J. Phys. Chem.*, 1993, 97; 10857-10861.
37. K.A. Janes, M.P. Fresneau, A. Marazuela, A. Fabra, M.J. Alonso. Chitosan nanoparticles as delivery systems for doxorubicin. *J. Cont. Rel.*, 2001, 73; 255-267.

38. P.P. Kleihues, D.N. Louis, B.W. Scheithauer, I.B. Rorke, G. Reifenberger, P.C. Burger, W.K. Cavenee. The WHO classification of tumors of the nervous system. *J. Neuropathol. Exp. Neurol.*, 2002, 61; 215-225.
39. S.C.J. Steinigeri, J. Kreuteri, A.S. Khalansky, I.N. Skidan, A.I. Bobruskin, Z.S. Smirnova, S.E. Severin, R. Uhl, M. Kock, K.D, Geiger, S.E. Gelperina. Chemotherapy of glioblastoma in rats using doxorubicin loaded nanoparticles. *Int. J. Cancer.*, 2004, 109; 759-767.
40. H.V Hoist, E. Knochenhauer, H. Blomgren, V.P. Collins, L. Ehn, M. Lindquist, G. Noren, C. Peterson. Uptake of adriamycin in tumour and surrounding brain tissue in patients with malignant gliomas. *Acta. Neurochir.*, 1990, 104; 13-16.
41. P.C. Merker, M.R. Lewis, M.D. Walker, E.P Richardson. Neurotoxicity of doxorubicin perfused through the cerebrospinal fluid spaces of the rhesus monkey. *Toxicol. Appl. Pharmacol.*, 1978, 44; 191-205.
42. S. Bennis, C. Chapey, P. Couvreur, J. Robert. Enhanced cytotoxicity of doxorubicin encapsulated in polyhexylcyanoacrylate nanospheres against multi-drug-resistant tumour cells in culture. *Europ. J. Cancer* 1994, 30; 89- 93.
43. H.S. Yoo, K.H. Lee, J.E. Oh, T.G. Park. In vitro and in vivo anti-tumor activities of nanoparticles based on doxorubicin-PLGA conjugates. *J. Cont. Rel.*, 2000, 68; 419-431.
44. A. Skladanowski, J. Konopa. Adriamycin and daunomycin induce programmed cell death (apoptosis) in tumor cells. *Biochem. Pharmacol.*, 1993, 46; 375-382.
45. J. Yuan, G. Murrell, A. Trickett, M.X. Wang. Involvement of cytochrome c release and caspase-3 activation in the oxidative stress induced apoptosis in human tendon fibroblasts. *Biochim. Biophys.*, 2003, 1641; 35-41.
46. S.S. Cameotra, R.S. Makkar. Recent applications of biosurfactants as biological and immunological molecules. *Curr. Opin. Microbiol.*, 2004, 7; 262-266.
47. A.P. Tulloch. The component fatty acids of oils found in spores of plant rusts and other fungi. *Can. J. Microbiol.*, 1964, 10; 359-364.
48. K.S. Bisht, R.A. Gross, D.L. Kaplan. Enzyme mediated regioselective acylations of sophorolipids. *J. Org. Chem.*, 1999, 64; 780-789.
49. A.P.J. Gorin, J.F.T. Spencer, A.P. Tulloch. Hydroxy fatty acid glycosides of sophorose from *Torulopsis magnoliae*. *Can. J. Chem.*, 1961, 39; 846-895.
50. I.M. Banat. Biosurfactants production and possible uses in microbial enhanced oil recovery and oil pollution remediation. *Bioresour. Technol.*, 1995, 51; 1-12.
51. M. Maingault. Utilization of sophorolipids as therapeutically active substances or cosmetic products, in particular for the treatment of the skin. U.S. patent **5,981,497**, 1999.

- 
52. K.J. Kim, D.S. Yoo, Y.B. Kim, B.S. Lee, D.D. Shin, E.K. Kim. Characteristics of sophorolipid as an antimicrobial agent. *J. Microbiol. Biotechnol.* 2002, 12; 236-241.
53. R. Gross, V. Shah. Antibacterial properties of various forms of sophorolipids. U.S. patent application no. **PCTIUS20031035871**, 2003.
54. R. Gross, V. Shah, D. Gustavo. Spermicidal and virucidal properties of various forms of sophorolipids. U.S. patent application no. **10/804778**, 2004.
55. V. Shah, G.F. Doncel, T. Seyoum, K.M. Eaton' I. Zalenskaya, R. Hagver, A. Azim, R. Gross. Sophorolipids, microbial glycolipids with anti-human immunodeficiency virus and sperm-immobilizing activities. *Antimicrob. Agents Chemother.* 2005, 49; 4093-4100.
56. R. Gross, V. Shah. Antifungal activity of various forms of sophorolipids. U.S. patent application no. **11/020683**, 2004.
57. E. Kandil, H. Zhang, R. Schulze, L. Dresner, M. Nowakowski, R. Gross, M.E. Zenilman. Sophorolipids block lethal effects of septic shock. *J. Am. Coll. Surg.*, 2003, 197; S40-S41.
58. C. Scholz, S. Mehta, K. Bisht, V. Guilmanov, D. Kaplan, R. Nicolosi, R. Gross. Bioactivity of extracellular glycolipids: Investigation of potential anti cancer activity of sophorolipids and sophorolipid derivatives. *Proc. Am. Chem. Soc.*, 1998, 39; 168-169.
59. C. Jing, S. Xin, Z. Hui, Q. Yinbo. Production, structure elucidation and anticancer properties of sophorolipid from *Wickerhamiella domercqiae*. *Enzyme Microb. Technol.*, 2006, 39; 501-506.
60. L.F. Sophia, S.R. Wallner, W.B. Bowne, M.D. Hagler, M.E. Zenilman, R. Gross, M.H. Bluth. Sophorolipids and their derivatives are lethal against human pancreatic cancer cells. *J. Surg. Res.*, 2008, 148; 77-82.
61. M. Kasture, S. Singh, P. Patel, P.A. Joy, A.A. Prabhune, C.V. Ramana, B.L.V. Prasad. Multiutility sophorolipids as nanoparticle capping agents: Synthesis of stable and water dispersible Co nanoparticles. *Langmuir* 2007, 23; 11409-11412.
62. S. Singh, P. Patel, S. Jaiswal, A.A. Prabhune, V. Ramana, B.L.V. Prasad. A direct method for the preparation of glycolipid metal nanoparticle conjugates: Sophorolipids as reducing and capping agents for the synthesis of water re-dispersible silver nanoparticles and their antibacterial activity. *New J. Chem.*, 2009, 33; 646-652.
63. R. Stupp, M.E. Hegi. Targeting brain-tumor stem cells. *Nat. Biotech.*, 2007, 25; 193-194.
64. Schreiner. Drug makers chase cancer stem cells. *Nat. Biotech.*, 2008, 26; 366-367.

65. R. Hong, N.O. Fischer, A. Verma, C.M. Goodman, T. Emrick, V.M. Rotello. Control of protein structure and function through surface recognition by tailored nanoparticle scaffolds. *J. Am. Chem. Soc.*, 2004, 126; 739-743.
66. H. Otsuka, Y. Nagasaki, K. Kataoka. PEGylated nanoparticles for biological and pharmaceutical applications. *Adv. Drug Delivery Rev.*, 2003, 55; 403- 419.
67. G.F. Paciotti, D.G.I. Kingston, L. Tamarkin. Colloidal gold nanoparticles: An novel nanoparticle platform for developing multifunctional tumor targeted drug delivery vectors. *Drug Dev. Res.*, 2006, 67; 47-54.
68. D. Shenoy, W. Fu, J. Li, C. Crasto, G. Jones, C. Dimarzio, S. Sridhar, M. Amiji. Surface functionalization of gold nanoparticles using hetero-bifunctional poly(ethylene glycol) spacer for intracellular tracking and delivery. *Int. J. Nanomedicine* 2006, 1; 51-57.
69. C.H. Wang, C.J. Liu, C.L. Wang, T.E. Hua, J.M. Obliosca, K.H. Lee, Y. Hwu, C.S. Yang, R.S. Liu, H.M. Lin, J.H. Je, G. Margaritondo. Optimizing the size and surface properties of polyethylene glycol (PEG) gold nanoparticles by intense X-ray irradiation. *J. Phys. D. Appl. Phys.*, 2008, 41; 195301- 195309.
70. T. Niidome, M. Yamagata, Y. Okamoto, Y. Akiyama, H. Takahashi, T. Kawano, Y. Katayama, Y. Niidome. PEG modified gold nanorods with a stealth character for in vivo applications. *J. Control. Rel.*, 2006, 114; 343- 347.
71. S. Aryal, J.J. Grailer, S. Pilla, D.A. Steeberb, S. Gong. Doxorubicin conjugated gold nanoparticles as water-soluble and pH-responsive anticancer drug nanocarriers. *J. Mater. Chem.*, 2009, 19; 7879-7884.
72. Y. Cheng, A.C. Samia, J.D. Meyers, I. Panagopoulos, B. Fei, C. Burda. Highly efficient drug delivery with gold nanoparticle vectors for in vivo photodynamic therapy of cancer. *J. Am. Chem. Soc.*, 2008, 130; 10643- 10647.
73. C. Park, H. Youn, H. Kim, T. Noh, Y.H. Kook, E.T. Oh, H.J. Park, C. Kim. Cyclodextrin covered gold nanoparticles for targeted delivery of an anti-cancer drug. *J. Mater. Chem.*, 2009, 19; 2310-2315.
74. W.S. Cho, M. Cho, J. Jeong, M. Choi, H.Y. Cho, B.S. Han, S.H. Kim, H.O. Kim, Y.T. Lim, B.H. Chung, J. Jeong. Acute toxicity and pharmacokinetics of 13 nm sized PEG coated gold nanoparticles. *Toxicol. Appl. Pharmacol.*, 2009, 236; 16-24.
75. P.R. Selvakannan, S. Mandal, S. Phadtare, R. Pasricha, M. Sastry. Capping of gold nanoparticles by the amino acid lysine renders them water dispersible. *Langmuir* 2003, 19; 3545-3549.

76. G. Zhang, Z. Yang, W. Lu, R. Zhang, Q. Huang, M. Tian, L. Li, D. Liang, C. Li. Influence of anchoring ligands and particle size on the colloidal stability and in vivo biodistribution of polyethylene glycol-coated gold nanoparticles in tumor-xenografted mice. **Biomaterials** 2009, 30; 1928-1936.
77. Y.J. Gu, J. Cheng, C.C. Lin, Y.W. Lam, S.H. Cheng, W.T. Wong. Nuclear penetration of surface functionalized gold nanoparticles. **Toxicol. Appl. Pharmacol.**, 2009, 237; 196-204.
78. D. Miyamoto, M. Oishi, K. Kojima, K. Yoshimoto, Y. Nagasaki. Completely dispersible PEGylated gold nanoparticles under physiological conditions: Modification of gold nanoparticles with precisely controlled PEG-6- polyamine. **Langmuir** 2008, 24; 5010-5017.
79. C.J. Sunderland, M. Steiert, J.E. Talmadge, A.M. Derfus, S.E. Barry. Targeted nanoparticles for detecting and treating cancer. **Drug Dev. Res.**, 2006, 67; 70-93.
80. M. Bergen, H.A.V. Recum, T.T. Goodman, A.P. Massey, S.H. Pun. Gold nanoparticles as a versatile platform for optimizing physicochemical parameters for targeted drug delivery. **Macromol. Biosci.**, 2006, 6; 506- 516.
81. J. Chen, X. Song, H. Zhang, Y.B. Qu, J.Y. Miao. Sophorolipid produced From the new yeast strain *Wickerhamiella domercqiae* induces apoptosis in H7402 human liver cancer cells. **Appl. Microbiol. Biotechnol.**, 2006, 72; 52-59.
82. Y. Liu, W.L. Lu, J. Guo, J. Du, T. Li, J.W. Wu, G.L. Wang, J.C. Wang, X. Zhang, Q. Zhang. A potential target associated with both cancer and cancer stem cells: A combination therapy for eradication of breast cancer using /inorelbine stealthy liposomes plus parthenolide stealthy liposomes. **J. Control. Rel.**, 2008, 129; 18-25.
83. L.M. Bareford, P.W. Swaan. Endocytic mechanisms for targeted drug delivery. **Adv. Drug Delivery Rev.**, 2007, 59; 748-758.
84. M. Song, X. Wang, J. Li, R. Zhang, B. Chen, D. Fu. Effect of surface chemistry modification of functional gold nanoparticles on the drug accumulation of cancer cells. **J. Bio. Mat. Res. Part A.**, 2007, 86A, 942- 946.